Chapter 2
Introduction: From Biological Experiments to Mathematical Models

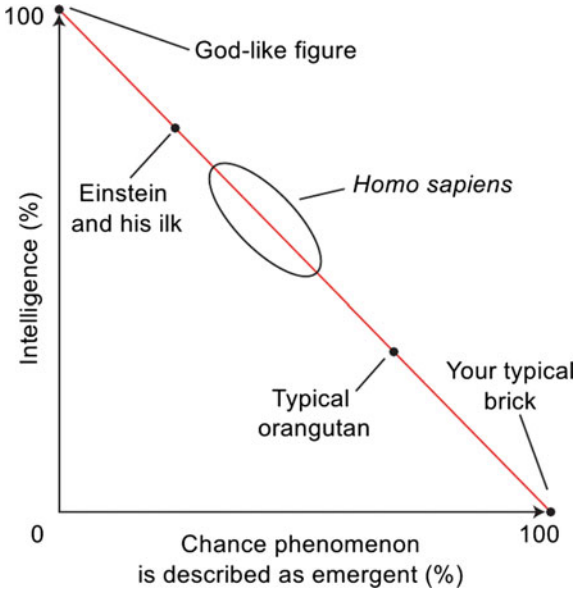

Bruce C. Gibb, The emergence of emergence, 2011

At first glance, scientists seem to have needed a surprisingly long amount of time to find the physical correlate of thought. While the brain itself, as an organ, has long been considered the seat of the mind,[1] it was only at the turn of the 20th century that Cajal and Golgi established the "neuron doctrine"—the hypothesis that the neuron is the fundamental functional unit of the brain. In the light of much earlier achievements in the physics of small scales, such as Bernoulli's kinetic theory of gases in the early 18th century, this comparatively slow development might appear paradoxical, especially given Hooke's and van Leeuwenhoek's discovery of the cell over two centuries before the discovery of the neuron. However, when considering the complexity of the "elementary" components involved, and moreover that of the emergent

[1]Notable exceptions include Aristotle, who believed it to be a blood-cooling device (Gross 1995).

M.A. Petrovici, *Form Versus Function: Theory and Models for Neuronal Substrates*, Springer Theses, DOI 10.1007/978-3-319-39552-4_2

phenomena, a theory of mind has to appear much less intuitive—and probably much less mathematically tractable—than thermodynamics.

Evidently, if we strive for more than just a phenomenological description of high-level information processing in the brain, we need to understand the functionality of its fundamental components. In this context, Sect. 2.1 represents as a brief introduction to the morphology and electrophysiology of neurons and synapses. In it, we review those processes in nerve cells that appear most relevant to information processing and communication. These "microscopic laws of motion" represent the fundamental building blocks for all theoretical and functional models that we discuss later on.

We should make clear that it happens with the mindset of a physicist when we follow such a reductionist approach. When we describe higher-level phenomena to "emerge" from low-level dynamics, there is no deus ex machina involved. When the whole becomes more than the sum of its parts, as is arguably the case for the brain, it is because a large ensemble of simple components exhibits features that are impossible to observe when only few such components interact. A useful description of such a system often involves the definition of new macroscopic variables, but they always represent a high-level view of a system that is entirely governed by fundamental interactions between its microscopic constituents.

Evolution is not equivalent to engineering and therefore its constructs, incrementally perfected over billions of years, always inherit vestiges of their predecessors, which might not necessarily serve a functional purpose. Additionally, all biological units need to perform metabolic and reproductive activities, for sustainment and growth, which massively add to their structural complexity. It is therefore quite likely that a rather high level of abstraction is sufficient (and probably even best suited) to understand information processing in neural networks. To which extent one can push this abstraction, however, remains an open question and subject to much debate among researchers in the field.

The requirement of abstraction, as well as a precise description thereof, is well-established throughout all physical sciences. It is the search for a minimal, but complete set of laws required to describe a given system that gives rise to the notion of a model. For the most part, a "model" is understood as synonymous to a "mathematical model" of a system, that is, a set of rules and parameters, preferably expressed as equations, which completely describe the dynamics of variables associated to the relevant properties of the system. This makes it possible to apply a vast array of mathematical tools and formalisms to analyze and predict its behavior. The unparalleled success of this approach has established it as the centerpiece of all natural sciences.

Building on the aforegoing electrophysiological considerations, Sect. 2.2 outlines the construction of several abstract models for neurons and synapses. The presented neuron models exhibit various levels of abstraction, particularly concerning the spike generation mechanism of neurons, which are crucial for the investigations described in Chaps. 4–6.

2.1 Morphology and Electrophysiology of Biological Neurons and Synapses

This section serves as a short overview of the biological mechanisms that underpin neuron and synapse dynamics. Understanding them is indispensable to formulating abstract models of neurons and synapses. For a much more in-depth view of the phenomena described here, we recommend Alberts et al. (1994) for the molecular biology topics and Gerstner and Kistler (2002) for the mathematical treatment.

2.1.1 Electrical Properties of the Cell Membrane

Just like every other cell, a neuron's interior is separated from the outside environment by the so-called plasma membrane. It consists mainly of a lipid bilayer, but also contains various (transmembrane) proteins which are essential for building up and dynamically changing a voltage across the membrane (Fig. 2.1).

While highly permeable to small neutral molecules such as water, the lipid bilayer itself is practically impermeable to ions and polar molecules, which are the main charge carriers in organic media, thereby effectively insulating the interior of the cell from its exterior. Due to its narrow width of roughly 5 nm, the membrane effectively acts as a capacitor, with a typical capacitance of $C_\mathrm{m} = 1\ \mu\mathrm{F/cm}^2$. For a patch of membrane with an area of $1\ \mu\mathrm{m}^2$, membrane voltage changes of several tens of mV can therefore be achieved by moving only several thousand monovalent ions across the membrane, about 3 orders of magnitude below the total number of ions in the cytosol. It is important to note that only those ions lying very close ($< 1\,\mathrm{nm}$) to the membrane influence its voltage, therefore any changes in the membrane potential need not affect ion concentrations in the rest of the cytosol.[2] This property is quintessential for enabling the high speed of neuron membrane potential dynamics required by real-world interaction and information processing—an aspect we shall return to later.

Cells make good use of their capability of establishing a gradient across their membrane, both chemical and electrical. Indeed, transmembrane gradients are the driving force of essentially all metabolic processes in the cell, especially solute transport and ATP synthesis.[3] However, the capability of the plasma membrane to

[2] Let us assume a neocortical pyramidal cell has a total area of $S = 3 \times 10^4\ \mu\mathrm{m}^2$ and a volume of $V = 10^4\ \mu\mathrm{m}^3$, with a specific membrane capacitance of $c = 1\,\mu\mathrm{F/cm}^2$ and a Na^+ concentration of $[\mathrm{Na}^+] = 3 \times 10^7$ ions/$\mu\mathrm{m}^3$. The number of ions required for an increase in membrane potential by 10 mV is then $N = cSU/e \approx 2 \times 10^7$, as compared to the total number of ions in the cell $N_\mathrm{tot} = [\mathrm{Na}^+]V = 3 \times 10^{11}$. This is only an approximate calculation, as estimates of cell sizes vary considerably, see e.g. Ambros-Ingerson and Holmes (2005).

[3] The quintessential question in the search for the origin of life is how this gradient could have appeared in early cell-like structures. Furthermore, while in prokaryotic cells, ATP is synthesized at the plasma membrane, in eukaryotes this process is taken over by specialized organelles—mitochondria and plastids. It has been argued that it was the acquisition of these organelles by early

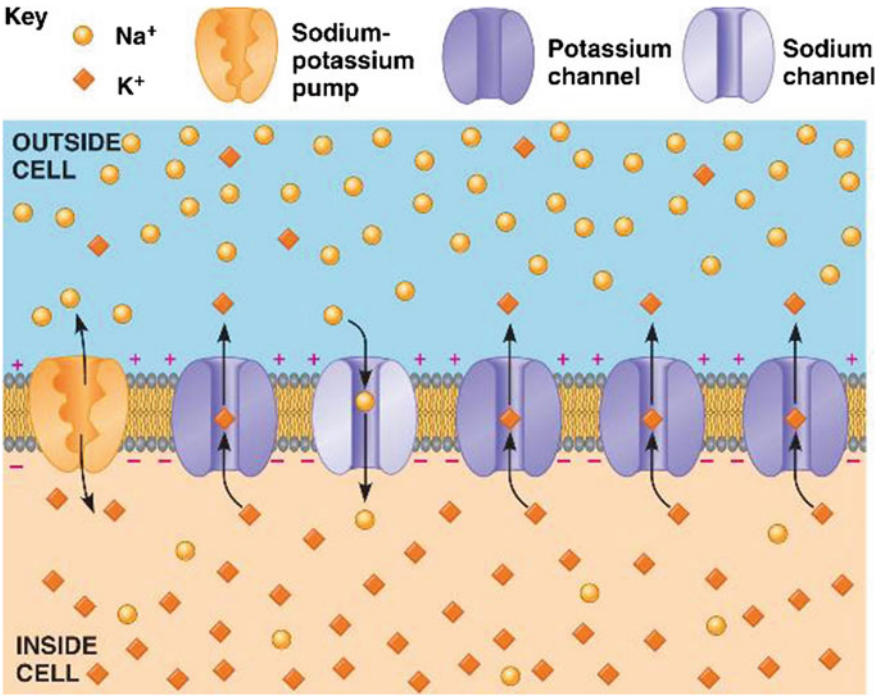

Fig. 2.1 Sketch of the plasma membrane, with embedded active pumps and leakage channels. See text for details. Image taken from expertsmind.com

maintain an electrochemical gradient is necessary, but not sufficient, to explain the existence of the gradient itself. The structure responsible for the (trans)membrane potential is the Na^+–K^+ pump.[4]

The Na^+–K^+ pump is an ATPase, a carrier protein embedded in the plasma membrane that hydrolyzes ATP to provide the energy for its operation. Within a full pump cycle, it transports 3 Na^+ ions from the cell plasma to the extracellular medium and 2 K^+ ions from the extracellular medium into the plasma. This leads to an excess of negative charge (or rather, a net total deficit of positive charge) inside the cell, which in turn translates to a negative membrane potential. As the electrochemical gradient increases, the pumping process becomes less efficient and the membrane potential reaches some equilibrium value.

(Footnote 3 continued)
prokaryotes that enabled the evolution of complex life. For an excellent discussion on these topics, we refer to Lane and Martin (2010, 2012).

[4] Actually, an electrochemical gradient would exist even without the Na^+–K^+ pump, due to the high concentration of organic compounds inside the cell. These, in turn, cause a high intracellular osmolarity, which would force water to move into the cell by osmosis. The Na^+–K^+ pump counters this potentially destructive effect by increasing the net extracellular concentration of inorganic ions.

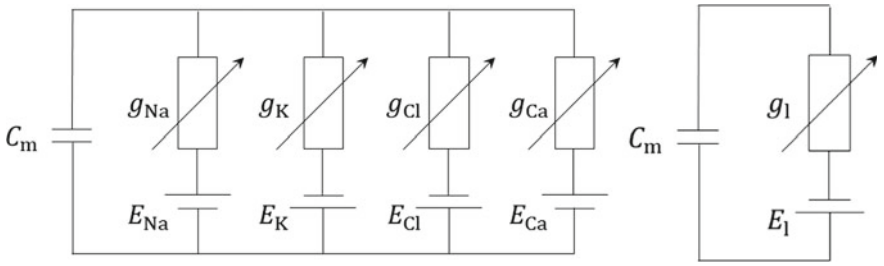

Fig. 2.2 *Left* full equivalent circuit of a cell membrane, with different ion concentrations acting as batteries. The Na^+ and K^+ batteries are governed by the Na^+–K^+ pump and the K^+ leakage channel, as described in the text above. Na^+ leakage channels also exist (see Fig. 2.1), but are much fewer in number (with a ratio of about 1:100 with respect to K^+ leakage channels). The two other ions that have significant contributions to the membrane potential are Ca^{++} and Cl^-, which have their concentrations regulated by similar pumping and leakage mechanisms. *Right* reduced equivalent circuit, with all ion concentrations condensed into a single battery and conductance

The activity of Na^+–K^+ pumps alone, however, would only account for about a tenth of the measured equilibrium value of some $-70\,\text{mV}$. A second type of transmembrane protein plays an essential role here: the K^+ leakage channel. This channel protein is permanently "open" and only allows the passage of K^+ ions. Because of the high concentration of potassium inside the cell, due to the Na^+–K^+ pump, an outflow of K^+ ions is established, that pulls down the membrane potential even further. This happens until an equilibrium value is reached, the so-called Nernst potential, the value at which diffusive and electrical forces counterbalance:

$$E_X = \frac{RT}{zF} \ln \frac{[X]_{\text{ext}}}{[X]_{\text{int}}}, \tag{2.1}$$

where R is the universal gas constant, F the Faraday constant, T the absolute temperature, z the charge of the ion in question X and $[X]_{\text{ext/int}}$ its extracellular and intracellular concentrations, respectively. However, various ions tend to have different Nernst potentials, due to their different charges and concentrations, hence the resting membrane potential becomes something like a weighted mean thereof.

Figure 2.2 shows the equivalent circuit that determines the resting potential V_{rest} of the membrane. Taking into account only the contributions from monovalent ions,[5] V_{rest} can then be calculated from the Goldman–Hodgkin–Katz (GHK) equation.[6] :

$$V_{\text{rest}} = \frac{RT}{F} \ln \frac{\sum_i P_{X_i^+} [X_i^+]_{\text{ext}} + \sum_i P_{Y_i^-} [Y_i^-]_{\text{int}}}{\sum_i P_{X_i^+} [X_i^+]_{\text{int}} + \sum_i P_{Y_i^-} [Y_i^-]_{\text{ext}}}, \tag{2.2}$$

[5] For ions of higher valence, such as Ca^{++}, extensions to the GHK equation exist—see, e.g., Pickard (1976). However, since during resting conditions, both the permeability and the concentration of Ca^{++} ions is comparatively low, calcium does not play a significant role in defining V_{rest}.

[6] Permeability and conductance are closely related, but not equivalent Channel conductance is, in particular, strongly voltage dependent. For a detailed discussion, see, e.g., Schultz et al. (1996).

with P_X denoting the permeability of the membrane to the ion type X. For a single ion type, it can be easily seen how the Nernst equation is merely a special case of the more general GHK equation. Because the membrane permeability to K^+ is usually at least an order of magnitude above the permeabilities to all other ion types, V_{rest} lies rather close to the K^+ reversal potential, which usually lies around $-80\,\text{mV}$.[7]

At this point, we can reduce the equivalent circuit from Fig. 2.2 to a simple RC circuit, with a single battery defining the rest or leak potential (here, as well as in most abstract neuron models, V_{rest} and E_l can be used interchangeably) as calculated from the GHK equation (Fig. 2.2). The term "leak potential" stems from the intuitive picture that following any temporary external electric stimulation, the capacitor leaks charges into the battery and reverts to its rest potential along an exponential curve. Indeed, the associated ODE of the membrane potential can be easily derived from Ohm's law in the reduced equivalent circuit:

$$C_m \frac{du}{dt} = g_l(E_l - u) + I, \tag{2.3}$$

where I stands for any external current source. The variable $\tau_m = C_m/g_l$ is called the membrane time constant and quantifies the speed at which the membrane potential reacts to external stimuli. This characteristic variable can be found in virtually any abstract neuron model. See Sects. 2.2 and 4 for a much more detailed discussion of membrane potential dynamics.

We now have a good mathematical model for the membrane potential of a cell in its resting state. Note that until this point, we have not yet addressed excitable cells (in particular, neurons), so the above considerations are, in principle, valid for any biological cell.

The above model also accounts for membrane dynamics under external current stimulation, albeit while implicitly neglecting the spatial extent, i.e., the 3D structure of the cell. It is extremely important to keep in mind that point models invariably limit the computational power of the units modeled as such. Also, for all point models, any claims of biological plausibility need to be reviewed carefully, especially since many neuron types have a very distinct branching structure. While most models and methods considered throughout this thesis do not take the spatial structure of the cells involved into consideration, we will address this issue briefly both from a theoretical perspective (Sect. 2.1.4), as well as in the case of a concrete cortical network model (Sect. 5.3).

[7] To get a feeling of the relevant variables, a numerical example is in order. For that, we consider measurements of the squid giant axon from Hodgkin (1958). The values given by Hodgkin read: $P_{Na^+} = 1$, $P_{K^+} = 100$, $P_{Cl^-} = 10$ (permeabilities are given relative to P_{Na^+}), $[K^+]_{ext} = 20$, $[K^+]_{int} = 200$, $[Na^+]_{ext} = 440$, $[Na^+]_{int} = 50$, $[Cl^-]_{ext} = 540$, $[Cl^-]_{int} = 40$ (ion concentrations given in mmol/l). At a temperature of 37 °C, the Nernst potentials then read $E_{Na^+} = 58.1$, $E_{K^+} = -61.5$ and $E_{Cl^-} = -69.6$, with the equilibrium membrane potential lying at $E_l = -58.6$ (potentials given in mV).

2.1.2 Action Potentials and the Hodgkin–Huxley Neuron Model

Just like all other cells, excitable cells establish an electrochemical transmembrane gradient for metabolic reasons. In addition to that, however, evolution has provided them with ways of manipulating their membrane potential, thereby allowing much faster communication and computation than would normally be possible through chemical diffusion processes. While many types of excitable cells exist, which also play an essential role in information processing (such as receptor cells or myocytes), the particular class of excitable cells we are interested in here are the neurons in the central nervous system.

Neurons do not exchange information permanently.[8] Their communication is mediated by all-or-nothing events, so-called action potentials (APs), or simply spikes. These are large pulses in the membrane potential with an amplitude of about 100 mV and a typical duration of several ms.

As a rough approximation, it can be said that action potentials occur when the membrane potential of a neuron increases beyond a certain value (usually around −50 mV). The membrane then spontaneously depolarizes, usually exceeding 0 mV, after which it quickly hyperpolarizes, even dropping below its resting potential for several ms. During this hyperpolarized state, also called the refractory phase, even strong stimuli can not initiate a second AP.

These phenomenological findings can be explained by another class of transmembrane proteins: voltage-gated ion channels. This hypothesis (later confirmed by Erwin Neher and Bert Sakmann, Nobel Prize 1991), along with a stochastic description of their dynamics, has earned Alan Lloyd Hodgkin and Andrew Huxley the 1963 Nobel Prize. The Hodgkin–Huxley model consists of a set of four differential equations and remains the most accurate model of neuronal membrane dynamics to date.[9]

Similar to leakage channels, voltage-gated ion channels only allow the passage of specific ion types. However, their conformation changes as a function of the membrane potential, thereby affecting their permeability. In a simplified picture,[10] these transmembrane proteins can be thought of as having "gates" which open and

[8] This is, of course, not absolutely true, since mechanisms such as local ion depletion, neurotransmitter diffusion or electrical crosstalk do enable additional communication pathways between neurons. Furthermore, electrical synapses (see Sect. 2.1.3) can also create a continuous link between membrane potentials.

[9] Modern extensions of the original model mainly include the addition of other types of ion channels and the morphology of neural cells.

[10] We have to stress that the Hodgkin–Huxley model is purely phenomenological and that the "gates" referenced multiple time in the text are only a mechanistic interpretation of the integer exponents in the gating variable equations. This is, however, quite close to reality: voltage-sensitive transmembrane proteins have, indeed, multiple identical compartments that change their conformation depending on the membrane potential. The voltage dependence of channel protein conformations is still the subject of intensive research, see, e.g., Long et al. (2007) for recent results on the structure of voltage-gated K^+ channels.

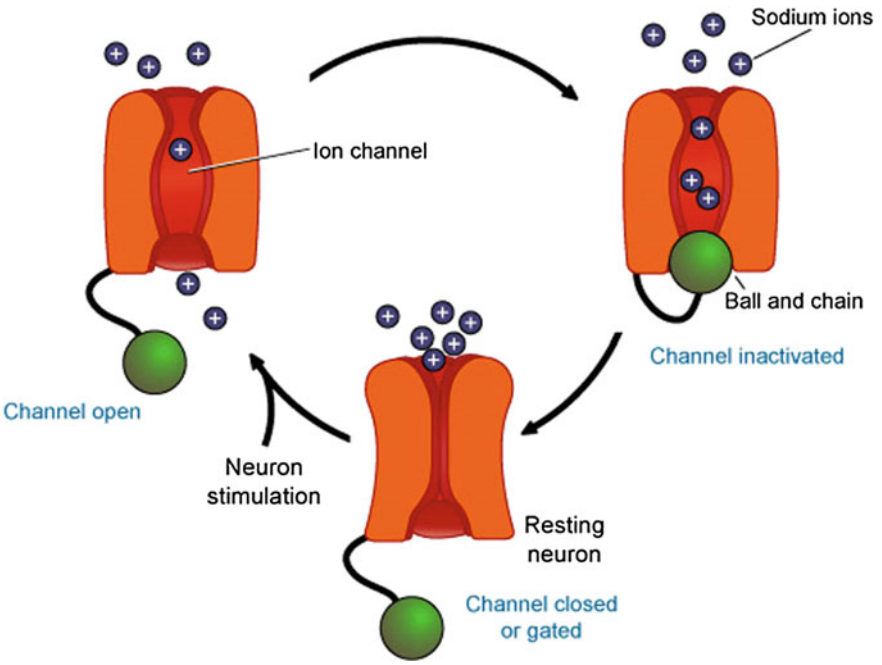

Fig. 2.3 Ball-and-chain model of a voltage-gated Na^+ channel. Upon excitatory stimulation of the neuron, its membrane potential increases, thereby (stochastically) triggering an opening, or activation, of the channel protein. The resulting influx of Na^+ ions increases the membrane potential even further, which causes even more Na^+ channels to open. This feedback loop continues until the "ball-and-chain" components of the molecule, which also react to high membrane voltages, but on a slower timescale, block the channel, thereby inactivating it. Note the difference between inactivation, which is an active self-blocking of ion channels, and deactivation, which is the process by which, when the membrane potential shifts outside the range that caused the channels to open in the first place, they simply close again. The latter is exactly what happens with voltage-gated K^+ channels in the Hodgkin–Huxley model, following a spike (see text for details). Image courtesy of Penn State Department of Biology

close stochastically, depending on the membrane potential. Figure 2.5 sketches several possible states for the Na^+ and K^+ voltage-gated ion channels. Both channel proteins have four gates, with the Na^+ channel possessing two different types of gate.[11] If we denote the probabilities of the three gate types being open by m, h (for Na^+) and n (for K^+), respectively, and the maximum conductance of the ion channels (in a fully open state) by g_{Na^+} and g_{K^+}, then the average currents flowing through the two ion channels read

[11] More recent studies from the 1990 s have shown that the K^+ channel also features several inactivation mechanisms of its own, one of which is similar to the ball-and-chain model of Na^+ inactivation from Fig. 2.3. See Kurata and Fedida (2006) for a review.

$$\langle I_{\mathrm{Na}^+} \rangle = g_{\mathrm{Na}^+} m^3 h (u - E_{\mathrm{Na}^+}) \quad \text{and} \tag{2.4}$$

$$\langle I_{\mathrm{K}^+} \rangle = g_{\mathrm{K}^+} n^4 (u - E_{\mathrm{K}^+}). \tag{2.5}$$

The voltage dependence of the gating variables m, h and n is given by

$$\dot{x} = -\frac{1}{\tau_x(u)}[x - x_0(u)], \quad x \in \{m, h, n\}, \tag{2.6}$$

with specific time constants $\tau_x(u)$ and equilibrium values $x_0(u)$. Alternatively, some authors prefer to use a somewhat different form of the above ODE:

$$\dot{x} = \alpha_x(u)(1 - x) - \beta_x(u)x, \quad x \in \{m, h, n\}, \tag{2.7}$$

with $x_0(u) = \alpha_x(u)/[\alpha_x(u)+\beta_x(u)]$ and $\tau_x(u) = 1/[\alpha_x(u)+\beta_x(u)]$. Figure 2.4 shows fits for $\tau_x(u)$ and $x_0(u)$ with the original parameters from Hodgkin and Huxley (1952).

Now we can return to the equivalent circuits from Fig. 2.2. For the sake of clarity, let us further assume that the leak and pump conductances—and thereby also g_{l}—are constant. We can now extend the reduced equivalent circuit by the voltage-gated Na^+ and K^+ channels described above. With Eqs. 2.4 and 2.5, the ODE for the membrane potential then becomes

$$C_{\mathrm{m}}\dot{u} = -g_{\mathrm{Na}^+} m^3 h (u - E_{\mathrm{Na}^+}) - g_{\mathrm{K}^+} n^4 (u - E_K) - g_{\mathrm{l}}(u - E_{\mathrm{l}}) + I \tag{2.8}$$

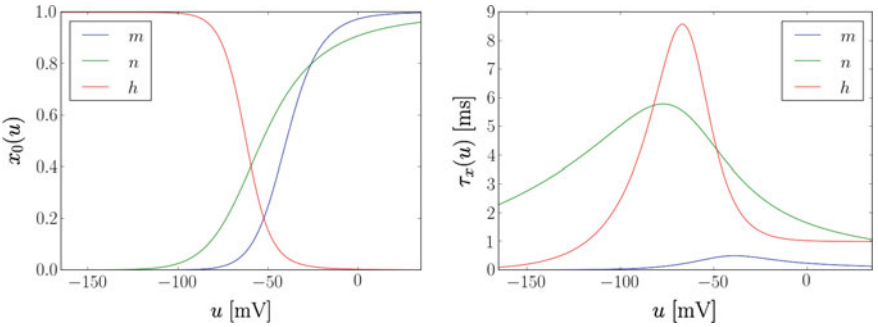

Fig. 2.4 Gating variables of the voltage-gated Na^+ and K^+ ion channels in the Hodgkin–Huxley model. *Left* equilibrium values as a function of the membrane potential u. Note how the m and n gates open at higher values of u, thereby activating the Na^+ and K^+ channels, respectively. Conversely, the h gates close for high u, thereby inactivating (i.e., actively closing) the Na^+ channels. *Right* time constants as a function of membrane potential u. Due to their fast dynamics (low time constant), the m channels open quickly, allowing the sharp onset of the action potential. Both the inactivation of the Na^+ channels via the h gates and the activation of the K^+ channels via the n gates occur on a slower timescale, jointly causing the falling flank of the action potential

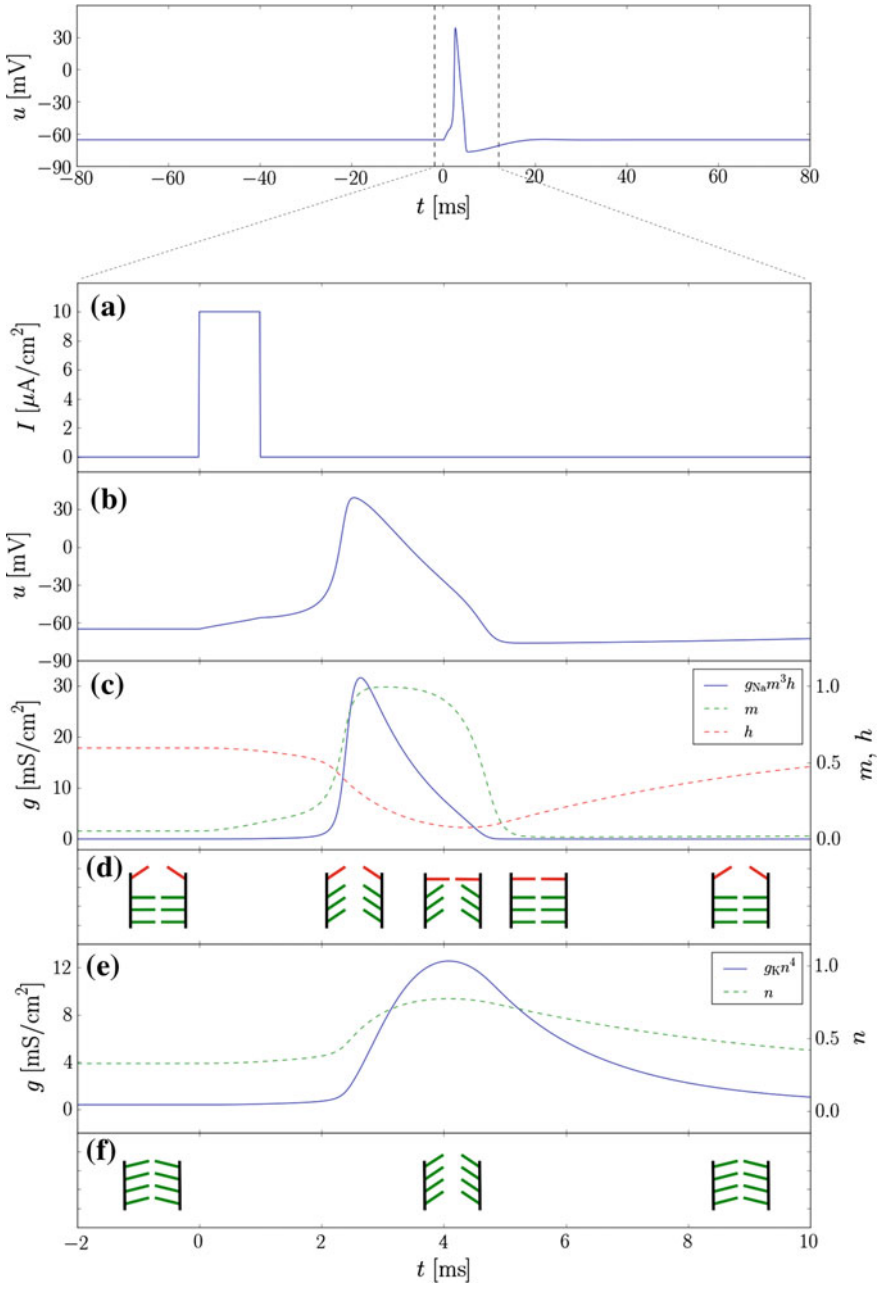
u [mV]
t [ms]
(a)
I [μA/cm²]
(b)
u [mV]
(c)
g [mS/cm²]
$g_{Na}m^3h$
m
h
m, h
(d)
(e)
g [mS/cm²]
$g_{K}n^4$
n
(f)
t [ms]

◀ **Fig. 2.5** Spiking dynamics in the HH neuron model. *Top* membrane potential during a single spiking event caused by a short step current stimulus at $t = 0$ ms. *Bottom* zoom-in on the time axis during the AP showing the evolution in time of all the relevant dynamic variables. **a** Current stimulus. **b** Membrane potential. The initially small change of $\approx 10\,\mathrm{mV}$ caused by the current stimulus results in a fast opening of the voltage-gated Na^+ channels which is strong enough to trigger a cascade effect that ultimately results in the rising flank of the AP. After the peak voltage is reached, inactivation of the Na^+ channels and activation of the K^+ channels causes the membrane potential to drop below the leak potential and slowly return to the resting state. **c** Evolution of Na^+ channel conductance (*solid curve*) and gating variables (*dashed curves*). The fast activation due to the *m* gates (*in green*) is followed by a slower inactivation due to the *h* gates (*in red*). This difference in time constants allows the sharp onset of the AP. Together with the activation of the K^+ channels (*n* gates, see panel **e**), the inactivation of the Na^+ channels is responsible for the refractory period that follows the AP. **d** Gate configuration of Na^+ channels. This is only a symbolic representation, since the conformational changes of the proteic subunits that build up individual gates are stochastic processes. **e** Evolution of the K^+ channel conductance (*solid curve*) and gating variable (*dashed curve*). The slower dynamics of the *n* gates as compared to the *m* gates allows the buildup of the AP before the decay towards the K^+ reversal potential. Note the long tail of the K^+ conductance compared to the Na^+ conductance. **f** Gate configuration of K^+ channels. As in panel **d**, this is only a symbolic representation. For the full set of parameters used for this simulation, see Tables A.1 and A.2

The four ODEs given by Eqs. 2.6 and 2.8 fully define the Hodgkin–Huxley neuron model.

Let us take a look at the dynamics of this model, with Fig. 2.5 serving as graphical guidance. The parameters used in this simulation are given in Tables A.2 and A.1. Without external stimulus, the membrane potential is at rest and does not change in time. Note that in the HH model, the rest potential is *not* equal to the leak potential E_l, but lies significantly lower, due to the K^+ channels always being open with nonzero probability. The Na^+ and K^+ voltage-gated channels are predominantly closed, or deactivated, due to the *m* and *n* gates, respectively. Upon stimulation with a strong enough step current, the *m*-gates start opening, activating the Na^+ channels and allowing an influx of Na^+, thereby increasing the membrane potential even further and leading to a cascade effect that pulls the membrane potential close to E_{Na^+}. This represents the steeply rising flank of the action potential. Due to their slower dynamics ($\tau_h \gg \tau_m$, see Fig. 2.4), the inactivation of the Na^+ channels via the *m* gates becomes dominant only with a certain delay, thereby not interfering with the sharp action potential onset.

If only Na^+ channels were present, the membrane potential would now slowly ($\tau_\mathrm{m} = C_\mathrm{m}/g_\mathrm{l} \approx 10\,\mathrm{ms}$) decay towards E_l. However, on roughly the same timescale as the inactivation of the Na^+ channels, the activation of the K^+ channels occurs.[12]

[12] Note that already in the deactivated state, individual *n* gates have a significant probability ($p \approx 0.3$) of being open. However, for a channel to be permeable, all gates have to be open at the same time, the probability of which scales with p^4 and is therefore much lower.

These quickly pull the membrane potential back down towards E_{K^+}, thereby generating the steep falling flank of the action potential. Again, due to their slow dynamics, the h gates remain closed and the n gates remain open for some time, leading to the relatively long characteristic "undershoot" of the membrane potential following the sharp spike. During this so-called refractory period, another spike is difficult to elicit, due to both the Na^+ channels being inactivated and the K^+ channels being open.

Apart from spiking when receiving strong and fast enough stimulation, HH neurons exhibit some other very interesting and maybe even surprising dynamics, which will be of particular interest later on, when we formulate more abstract neuron models. Whether these features are of any computational relevance is an important topic of ongoing debate.

Let us first turn our attention towards the "spiking threshold". Does there exist a value of the membrane potential which, once reached, guarantees that the neuron will spike? As we can see from Eq. 2.8, one can control the equilibrium value of the membrane potential by varying the external input current I, thus allowing to define a "threshold current" that is analogous to a threshold potential, should one exist. Medical dictionaries define the so-called rheobase as the minimal electric current required to excite a tissue given an indefinitely long time during which the current is applied.

Figure 2.6 shows an HH neuron stimulated with a step current which is strong enough to trigger persistent spiking while it remains on. Following its definition, one must assume that the rheobase is smaller or equal to the applied stimulus. However, if one increases the input current slowly, even at double the value of the previous stimulus, no spike is triggered. Indeed, if the input current is increased slowly enough,

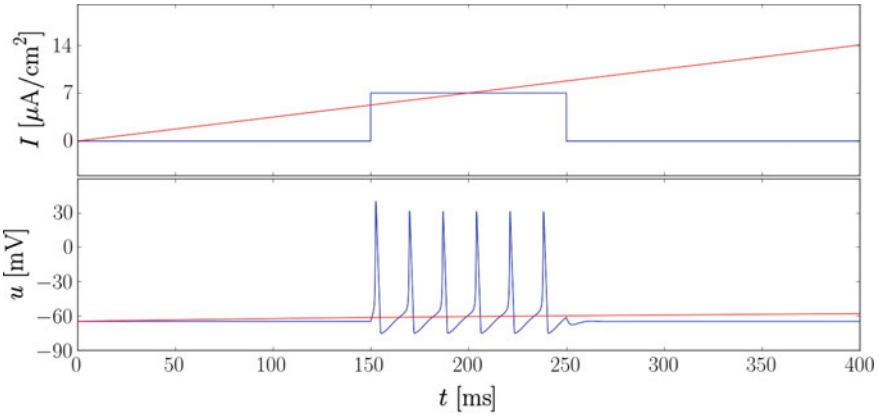

Fig. 2.6 Searching for the rheobase of an HH neuron (and not finding it). When stimulated with a step current of 7 pA/cm^2, the neuron goes into a regular spiking mode (*blue curves*). If one increases the current slowly enough, one can reach double that value (and, in principle, any value) without triggering a spike response (*red curves*)

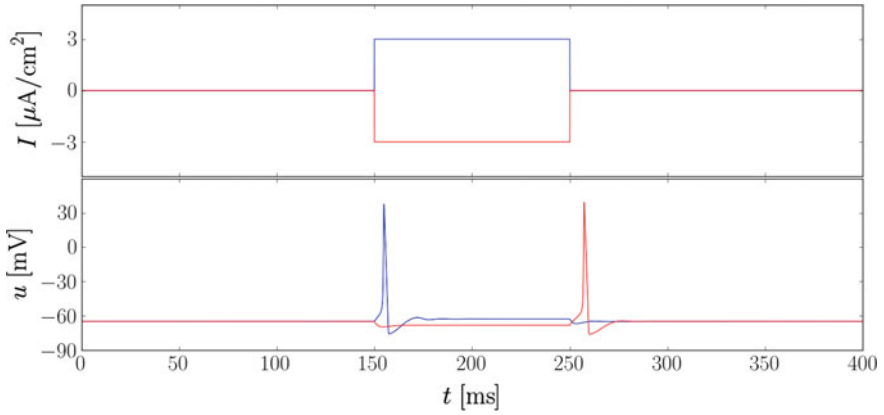

Fig. 2.7 Inhibitory rebound of an HH neuron. Given a high enough amplitude, both excitatory (*blue curves*) and inhibitory (*red curves*) stimuli can cause a spike in the HH model, if their onset (in the excitatory case) and end (in the inhibitory case) are quick enough

one can converge smoothly to any membrane potential value. Even for step currents, there is no clear threshold for which spiking is initiated. When decreasing the step value with fine enough granularity, the neuron responds with an increasing delay, with a spike of decreasing amplitude (not shown here).

This goes to show that HH neurons do not have a firing threshold in the precise mathematical sense. While the threshold assumption may be a very practical one,[13] as we shall discuss later in Sect. 2.2.1, it is important to keep in mind that it is a mathematical abstraction of an otherwise different physical phenomenon. In compliance with common terminology, we will nevertheless use the terms "suprathreshold" and "subthreshold" when describing regimes where a neuron fires or does not fire, respectively.

Another interesting phenomenon is the so-called (post-)inhibitory rebound. When stimulated (inhibited) by a negative current, the membrane potential naturally drops below E_l. If the stimulation ends abruptly and the inhibitory current was long and strong enough, a single spike can be elicited (Fig. 2.7). The explanation for this behavior lies again in the difference between the time constants of gate dynamics. The temporarily low membrane potential results in a stronger deactivation of the K^+ channels (n gates) and a weaker inactivation of the Na^+ channels (h gates). Upon the abrupt termination of the inhibitory stimulus, the membrane is pulled back towards E_l, but the fast m gates open quicker than the other two gate types can react to the change in voltage, causing an overshoot, which, when large enough, leads to spiking.

This effect is impossible to account for in neuron models governed by a single, first-order ODE, which possess a resting potential (stable fixed point of u). The extremely popular LIF model, discussed in detail in Sect. 2.2.1.1, is one such

[13] See also Kistler et al. (1997) for a similar discussion related to a different type of simplified neuron model (the spike-response model).

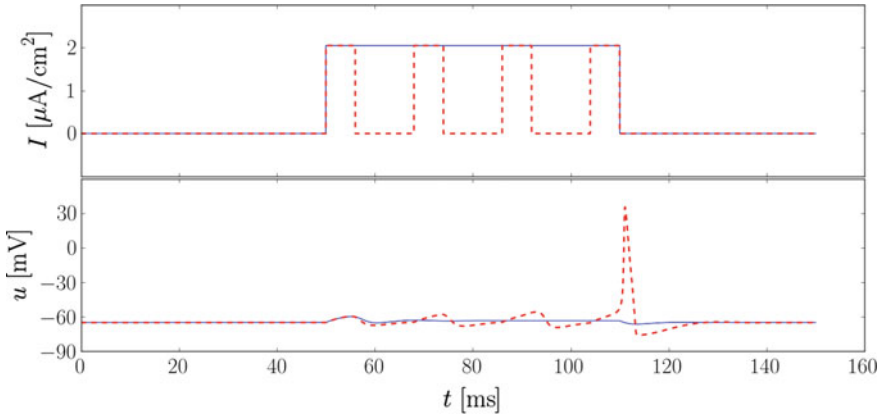

Fig. 2.8 Resonance phenomenon in the HH model. If an excitatory stimulus is too weak, it may not trigger a spike (*blue curves*). However, a pulsed stimulus with the same amplitude and correct frequency (which depends on the model parameters, especially the gating variable time constants), can cause a resonance phenomenon where the driven oscillations of the membrane lead to an AP

example. This is one of the reasons why neuron models of intermediate complexity have been developed and are being used for modeling cortical function. We point to Sects. 2.2.1.2, 3.3.1 and 5.5 for further elaboration on this topic.

The third and final phenomenon we shall address here is resonance. It is similar to the inhibitory rebound in that it is also caused by the different timescales on which gate dynamics evolve and it can also not be reproduced with first-order, single-ODE models. When stimulated periodically with a current of an amplitude that would otherwise not elicit a spike, an HH neuron can be provoked to fire, as shown in Fig. 2.8. This happens only if the pulse frequency of the stimulus is close to a specific value for the given neuron, hence the denomination of the effect. As shown in e.g. Izhikevich (2007), in vitro recordings of cortical neurons also show rebound and resonant spiking.

2.1.3 Synapses

After having discussed the individual dynamics of the fundamental building blocks of neural networks, we now turn to the other key ingredient in neural information processing: the interneuron interaction.

When the membranes of two neurons lie in close proximity to each other,[14] a so-called synapse can form, enabling the transmission of electrical signals between the two cells. Through a synapse, a spike of the presynaptic neuron can elicit a temporary

[14]More precisely, where the axon of the presynaptic cell touches a dendrite of the postsynaptic cell. See Sect. 2.1.4 for more details on neuron morphology and its functional consequences.

change in the membrane potential of the postsynaptic cell called a PSP.[15] Depending on whether the PSP has a positive (excitatory) or negative (inhibitory) influence on the membrane potential, it is also called an EPSP or an IPSP, respectively. Two fundamentally different types of synapses exist: electrical and chemical ones.

Electrical synapses are very simple in their structure. In an electrical synapse, the neuron membranes are separated by a narrow space called a gap junction or synaptic cleft, which is several nm wide. At the site of the gap junction, the membranes contain numerous junction channels called connexons, which can be thought of simply as pores that connect the cytoplasm of the two cells. These channels are wide enough to allow the passage of all relevant charged ion types (among others), thereby enabling the passive flow of ionic currents and thus the transmission of electrical signals. Electrical synapses are therefore very fast, with synaptic delays (time lag between the arrival of the presynaptic spike and the onset of the PSP) on the order of 0.2ms. They also allow signal transmission in both directions. However, despite their distinct speed advantage, they only represent a distinct minority of synapses in the neocortex. One reason might be that due to their simple structure, they lack the versatility and plasticity of chemical synapses (Fig. 2.9).

Chemical synapses, on the other hand, have a distinctly asymmetric structure. The presynaptic terminal, or synaptic bouton, contains specialized transmission molecules called neurotransmitters. These are enclosed in so-called vesicles, spherical formations about 40 nm in diameter surrounded by a plasma membrane. Vesicle membranes contain a particular type of protein which, when activated by Ca^{++} ions, causes the fusion of the vesicle to the cell membrane. When the presynaptic cell fires, the AP causes the opening of voltage-gated Ca^{++} channels, thereby creating an influx of Ca^{++} ions into the synaptic bouton. The resulting high Ca^{++} concentration causes the vesicles lying in the proximity of the cell membrane to fuse with it, releasing their contents into the synaptic cleft. The released neurotransmitters can now freely diffuse throughout the synaptic cleft, which is about 20 nm wide, reaching the postsynaptic terminal within several ms (and making chemical synapses an order of magnitude slower than electrical ones). At the postsynaptic terminal, the target neuron membrane contains a high density of receptor proteins called ligand-gated ion channels, which change their conformation in the presence of particular molecules. The neurotransmitter molecules cause the opening of these ion channels, creating an influx of charged ions into the postsynaptic cell. Formally, this amounts to an increase in (postsynaptic) membrane conductance for a specific ion type and is consequently dubbed a PSC.[16] This, in turn, elicits a PSP on the postsynaptic membrane. Due to Brownian motion and enzymatic metabolization, the transmitter molecules eventually break loose from the receptors, returning them to a closed state and ending the PSC. The freed neurotransmitter molecules or their metabolites can

[15] Which stands for "postsynaptic potential" and is therefore a rather unfortunate acronym for something representing a temporary change in the latter.

[16] Coincidentally, the abbreviation "PSC" can stand for either postsynaptic current (generated by the influx of ions through the ligand-gated ion channels) or postsynaptic conductance. The reader is therefore encouraged to pay particular attention to the context in which this acronym appears.

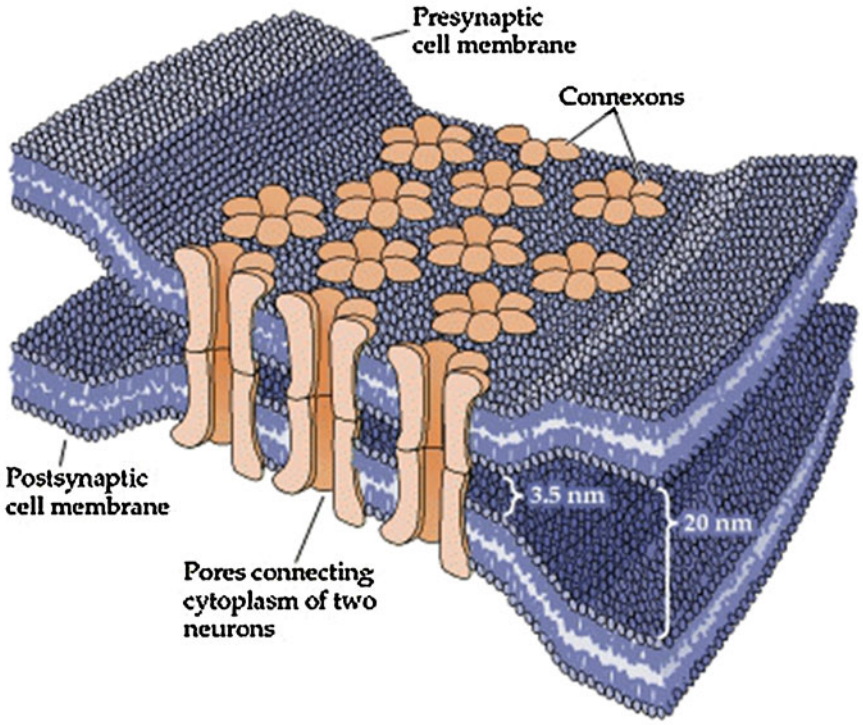

Fig. 2.9 Electrical synapse. In an electrical synapse, cell membranes are separated by an extremely narrow synaptic cleft. Special transmembrane proteins called connexons bridge the synaptic cleft and allow the passage of, among others, charged ions. Electrical excitations of the presynaptic membrane can thereby propagate passively to the postsynaptic membrane. Image taken from Purves et al. (2001)

then be reabsorbed and, if necessary, reconstituted by the presynaptic terminal and enclosed in new vesicles, thereby becoming available for future release (Fig. 2.10).

If multiple spikes arrive in close succession, their effects on the membrane conductance/current are summed up (aside from short-term saturation/depletion mechanisms, which will be discussed in Sect. 2.2.2.2). The same is true for PSCs arriving from different synapses. Since the neural membrane integrates over its inputs, PSPs sum up as well, both temporally (over different spikes) and spatially (over different synapses).

The various steps and components of this complex chain of events have many profound functional consequences.

The use of neurotransmitters as intermediates requires their metabolization by the presynaptic neuron. Therefore, it appears reasonable that every neuron releases the same set of neurotransmitters at each of its efferent synaptic sites. This principle,

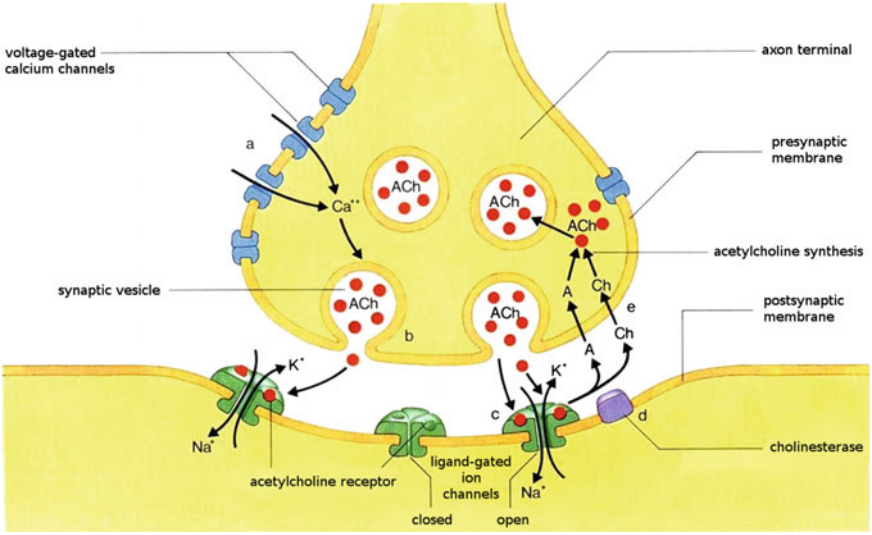

Fig. 2.10 Chemical synapse. When the presynaptic neuron fires, the elevated membrane potential at the presynaptic terminal causes voltage-gated Ca^{++} channels to open, creating an influx of Ca^{++} ions. These bind to vesicles containing neurotransmitter molecules, causing them to fuse with the cell membrane and spill their contents into the synaptic cleft. The diffusing neurotransmitters eventually reach the postsynaptic terminal, where they activate specific receptors in the postsynaptic cell membrane, which in turn allow the passage of charged ions, thereby eliciting a PSP. Eventually, the neurotransmitter molecules break loose from the receptors and are reabsorbed by the presynaptic cell for re-release. Image modified from Knodel (1998)

coined by John Eccles in 1954,[17] is known as Dale's law, and remains until today an important rule of thumb with only few known exceptions (Fig. 2.11).

The receptors activated by particular neurotransmitters are only permeable to specific ion types. Depending on whether channeled ions increase or decrease the neuron membrane potential, receptors can be classified as either excitatory or inhibitory. The two major neurotransmitters in the mammalian CNS are glutamate and GABA, which preferentially target excitatory and inhibitory receptors, respectively. Therefore, and as a corollary of Dale's law, depending on whether a neuron is glutamatergic or GABAergic, it can be either excitatory or inhibitory, but usually not both at the same time.

Given that communication at chemical synapses happens through diffusion, a fraction of the released neurotransmitter molecules can escape the synaptic cleft and diffuse freely into the intercellular medium. These can then affect neighboring

[17] There has been quite some historical controversy surrounding the precise wording of Dale's law. It concerns the ambiguity of the original statement from 1954 about whether one neuron may release multiple types of neurotransmitters at its terminals (Eccles et al. 1954). A revised version that is in compliance with today's knowledge has been formulated by Eccles in 1976: "I proposed that Dale's Principle be defined as stating that at all the axonal branches of a neurone, there was liberation of the same transmitter substance or substances" (Eccles 1976).

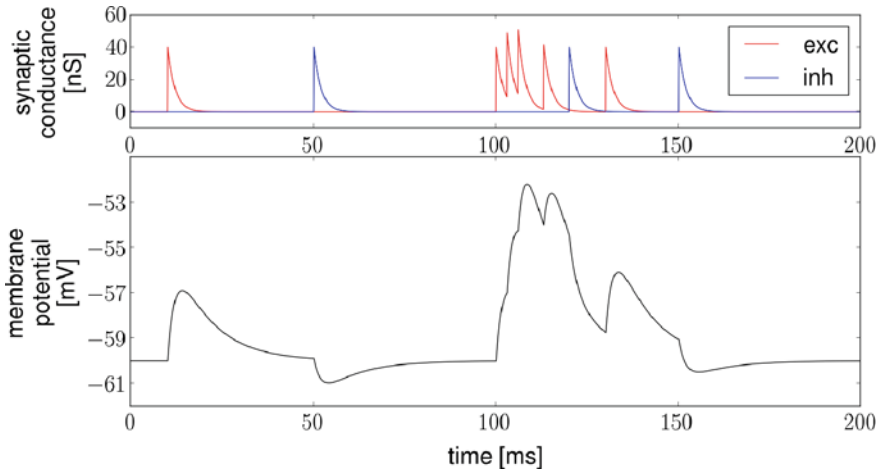

Fig. 2.11 Simulation of synaptic events. A single neuron is stimulated by an excitatory and an inhibitory presynaptic partner. Their spikes cause changes in the membrane conductance: *red* for excitatory (towards E_{Na^+}) and *blue* for inhibitory (towards E_{K^+}). Despite the two synapses having the same weight (as can be seen from the equal height of their PSCs), the inhibitory PSPs are significantly smaller than the excitatory ones due to the membrane potential lying much closer to E_{Na^+} than to E_{K^+}. When synaptic events arrive in quick succession, both temporal and spatial summation of their effects can be observed. Even when PSCs are too far apart to superpose, PSPs may still do so, due to the relatively long membrane time constant. A more detailed understanding of these phenomena, we point to the section on mathematical models of synaptic interactions (Sect. 2.2.2) and the analytical solution of the membrane potential equation (Sects. 4.2.1–4.2.4)

neurons non-synaptically in various ways, triggering complex metabolic pathways that may, in turn, cause profound changes in the dynamics of the neural network. This capability of neuromodulation gives chemical synapses far-reaching functional control over a wide range of temporal and spatial scales, much in contrast to their electrical counterparts.

Due to the complexity of the neurotransmitter release-reuptake-cycle, synaptic transmission can vary over time in various ways. It can either be subject to intrinsic dynamics, such as a gradual weakening of the synapse due to vesicle depletion, or be influenced externally by e.g. the firing of the postsynaptic neuron. This phenomenon, called synaptic plasticity, can obviously carry deep functional consequences for any network of spiking neurons. As such, it plays an essential role in learning, adaptation, memory formation etc., and is therefore a key component in neural modeling.

Because of their complexity, synaptic dynamics are rarely modeled in full detail. Especially when it comes to plasticity, models become increasingly phenomenological and less mechanistic. Many famous models of synaptic plasticity, such as the Hebb and BCM rules, have been originally formulated as firing-rate dependent and are therefore not easily implementable in spiking neural network models. Section 2.2.2 will address the modeling of synaptic transmission and plasticity in more detail.

2.1.4 Spatial Structure of Neurons

Until now, we have only considered the dynamics of structureless, pointlike neurons. The structure of neural cells is, however, important for two reasons. First and foremost, the structure of a neuron can have a profound impact on the way it processes inputs from other neurons. Secondly, the interplay of membrane morphology and electrochemistry leads to a preferred directionality in the transmission and processing of information.

A sketch of the functionally most relevant structural components of a neuron can be found in Fig. 2.12. A characteristic feature of a neuron is the branching tree of dendrites that grow out of the cell body or soma. Synaptic stimuli generate electrical excitations of the cell membrane that travel across the dendrites towards the soma. Projecting out of the soma is a single so-called axon, which is usually longer and thicker than the dendrites. At the junction between soma and axon, also called the axon hillock, the ion channel density is particularly high, making it the area most likely to trigger an AP. The AP then travels along the axon towards terminals connecting it, via synapses, to other neurons, through which it can impinge on their respective membranes.

An AP that has been initiated at the axon hillock can only move away from the soma, which we shall henceforth label as the forward direction. The reason for this lies within the very mechanisms that generate the AP described in the previous section.

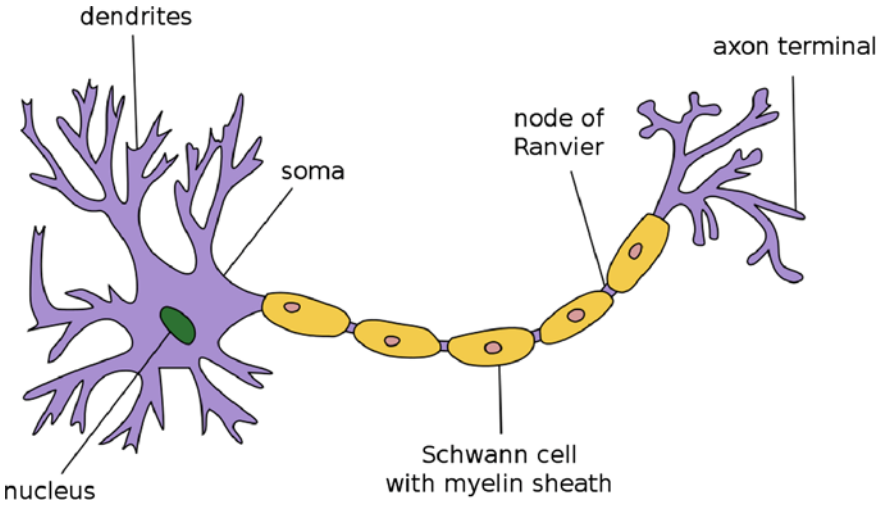

Fig. 2.12 Sketch of a neural cell. The cell nucleus resides in the cell body or soma. Thin, branching projections called dendrites gather information from afferent neurons. Spikes generated by this neuron are transmitted to efferent neurons via the axon, which is surrounded by a myelin sheath for faster signal transmission via saltatory propagation, from one node of Ranvier to the next. Dendrites of target neurons dock via synapses at the axon terminals. Modified from http://en.wikipedia.org/wiki/File:Neuron_Hand-tuned.svg

While the leading edge of the spike moves forward due to the activation of Na^+ channels, the trailing edge does so due to the inactivation of the Na^+ channels and activation of the K^+ channels. Thus, at any point in time, the membrane excitation can not move backwards due to the Na^+ channels towards the soma having already been inactivated.

Let us now consider a simple model for the propagation of electrical signals along the neural membrane. The so-called cable theory dates back to the work by Thomson (Lord Kelvin) from the 1850s, and was initially developed to model signal transmission in submarine telegraphic cables. We will not provide a full mathematical derivation here, since it is only of peripheral interest to the present work (see Sect. 5.3), and recommend Chap. 2.5 of Gerstner and Kistler (2002) instead, which features an in-depth discussion of the cable equations.

Neural cable theory assumes, in a first approximation, that all components of the neuron (dendrites, soma, axon) transmit electrical signals passively. The radius of the "neural cable" is modeled as constant and, at any point on the membrane, incident currents are assumed to sum up linearly. These are indeed very crude simplifications of neural electrophysiology,[18] but the mathematical tractability gained from sacrificing biological fidelity yields important insights into the effects of spatial structure on the propagation of electrical signals, which obviously has functional implications for neural information processing. We consider it crucial to accentuate this aspect, especially given the fact that, as we shall see later, network models very often do not take into account the full consequences of neural morphology.

In classical cable theory, the membrane acts as a sequence of infinitesimal RC circuits connected in parallel (Fig. 2.13). Here, $r_l dx$ represents the longitudinal resistive element and r_m/dx and $c_m dx$ the transversal resistive and capacitive elements, respectively. The latter are equivalent to $1/g_l$ and C_m, which have been discussed in Sect. 2.1.1. External currents that excite the membrane are subsumed under the notation $i^{ext}dx$. Note how the additive rules for resistors, capacitances and currents lead to the factors "$\cdot\, dx$" and "$/dx$", depending on whether they are connected in parallel or in series. The infinitesimal elements we use here are measured per membrane-length unit (and hence $[r_m] = \Omega\text{m}$, $[r_l] = \Omega/\text{m}$, $[c_m] = \text{F/m}$ and $[i^{ext}] = \text{A/m}$).

Without loss of generality, we can assume the resting potential of the membrane to be 0. The longitudinal current through the membrane $i(t, x)$ causes a voltage drop over the longitudinal resistance $r_l dx$ of

$$u(t, x) - u(t, x + dx) = i(t, x) r_l dx. \tag{2.9}$$

[18] As we have seen in Sect. 2.1.2, active (voltage-gated) channels on the membrane are a major component of membrane dynamics, even in the subthreshold regime. Dendrites also become thicker as they join and approach the soma, with the soma diameter being many times larger than that of distal dendrites. Finally, transmembrane currents do not sum up linearly, as the transmembrane proteins are not ideal resistors.

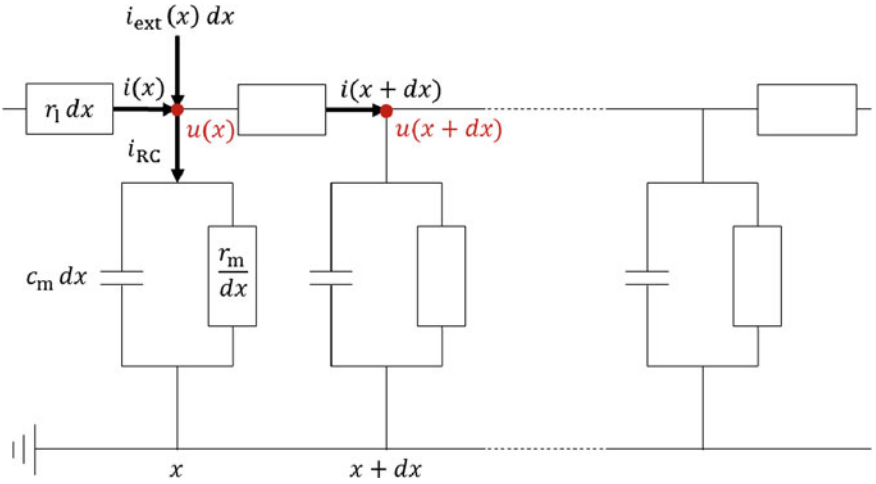

Fig. 2.13 The neuron membrane can be viewed as being composed of infinitesimal segments dx, each of which contains a longitudinal resistor $r_l dx$ and a leak circuit, which consists of a capacitor $c_m dx$ and a resistor r_m/dx connected in parallel. Due to gauge freedom one can set the voltage of the cell exterior, represented by the bottom horizontal wire, to zero (ground). The cable equation can be found by applying Ohm's law over the longitudinal resistive element and Kirchhoff's current law at a node along the inner cell membrane (top horizontal wire)

The current flowing through the infinitesimal RC circuit at point x is the sum of the current that charges the capacitance $c_m dx$ and the one flowing through the resistor r_m/dx:

$$i^{\text{RC}}(t,x) = c_m dx \frac{\partial}{\partial t} u(t,x) + \frac{u(t,x)}{r_m/dx}. \tag{2.10}$$

Conservation of current at point x demands that

$$i(t,x+dx) - i(t,x) - i^{\text{ext}}(t,x)dx + i^{\text{RC}} = 0. \tag{2.11}$$

In the limit of $dx \to 0$, we can rearrange equations such that we can substitute $\frac{u(t,x+dx)-u(t,x)}{dx}$ and $\frac{i(t,x+dx)-i(t,x)}{dx}$ by $\frac{\partial u(t,x)}{\partial x}$ and $\frac{\partial i(t,x)}{\partial x}$, respectively. As a final step, we can now substitute Eqs. 2.9 and 2.10 into Eq. 2.11 (and drop the arguments x and t for clarity). The cable equation describing this system then reads

$$\frac{1}{r_l}\frac{\partial^2 u}{\partial x^2} = c_m \frac{\partial u}{\partial t} + \frac{u}{r_m} - i^{\text{ext}}, \tag{2.12}$$

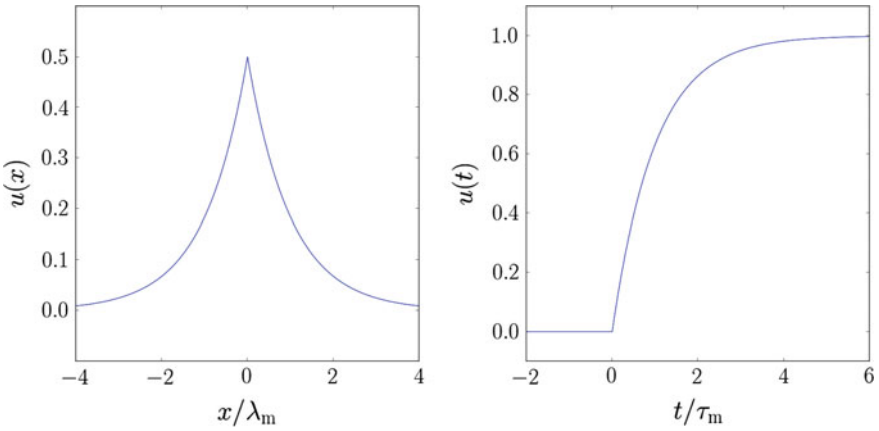

Fig. 2.14 Special solutions to the cable equation. The membrane potential is given in arbitrary units, as we are only interested in the shape of the curves. *Left* stationary solution with respect to time. A constant current is applied at a single point $x = 0$ along the membrane. The membrane potential decays exponentially as a function of distance to the point of injection, with a decay constant equal to the electrotonic length scale λ_m. *Right* stationary solution with respect to space. All points along the membrane receive the same current, which in this case is a step function at $t = 0$. The membrane potential decays exponentially towards the new equilibrium value, with a decay constant equal to the membrane time constant τ_m

By setting $\lambda_m = \sqrt{r_m/r_l}$ (the so-called electrotonic length scale) and $\tau_m = r_m c_m$ (the membrane time constant, see also 2.3), we can rewrite Eq. 2.12 as

$$\tau_m \frac{\partial u}{\partial t} - {\lambda_m}^2 \frac{\partial^2 u}{\partial x^2} + u = r_m i^{ext}, \tag{2.13}$$

Each of the two specific constants in this equation describes an intuitive property of the membrane Fig. 2.14. Assume, for instance, that we inject a constant current $i^{ext}(t, x) = \delta(x)/r_m$ at $x = 0$ and wait until the membrane potential does not change anymore in time. Equation 2.13 then becomes

$${\lambda_m}^2 \frac{\partial^2 u}{\partial x^2} = u - \delta(x) \tag{2.14}$$

and we can find the stationary solution

$$u(x) = \frac{1}{2} \exp\left(-\frac{|x|}{\lambda_m}\right). \tag{2.15}$$

It now becomes apparent that the electrotonic length scale λ_m is a measure of the attenuation of an input signal along the membrane. More precisely, it represents the length after which a stationary signal becomes weaker by a factor of $1/e$.

Similarly, if one injects a current homogeneously along the entire membrane, the spatial derivative in Eq. 2.13 vanishes and we are left with

$$\tau_{\mathrm{m}} \frac{\partial u}{\partial t} = -V + r_{\mathrm{m}} i^{\mathrm{ext}}, \tag{2.16}$$

which is exactly equivalent to the pointlike leaky neuron model by Eq. 2.3. For a constant current $i^{\mathrm{ext}}(t) = 1/r_{\mathrm{m}}\Theta(t)$, we can easily write down the solution

$$u(t) = \Theta(t)\left[1 - \exp\left(-\frac{t}{\tau_{\mathrm{m}}}\right)\right] \tag{2.17}$$

and see that the membrane time constant τ_{m} is a measure of the reaction speed of the membrane to changes in stimulus.[19] Similar to λ_{m}, it represents the time after which the membrane gets closer to its new equilibrium value by a factor of $1/e$.

We can now search for analytical solutions to the cable Eq. 2.13. In order to promote an intuitive understanding, we note how, although it appears here in the context of electrodynamics, this type of PDE is found in many areas of physics, including thermodynamics and quantum mechanics. It is closely related to e.g. the Fokker–Planck (a.k.a., depending on context, Smoluchowski) and Schrödinger equations. This already gives us a strong hint that dispersion (i.e., spreading of wave packets) plays an important role in the time evolution of membrane excitations. We need to stress, however, that the cable equation does not describe a diffusion process and is only formally similar to one. A detailed discussion of the Fokker–Planck equation as a formalization of a true diffusion process is, however, of central importance to the behavior of neurons driven by stochastic stimuli and shall be discussed in detail in the context of stochastic neural computation (Chap. 6).

The general approach to solving linear PDEs such as the cable equation is by using the Green's function formalism. For a generic linear PDE

$$\mathcal{L}u(t,x) = f(t,x) \tag{2.18}$$

with an arbitrary linear differential operator $\mathcal{L} = \mathcal{L}(x,t)$, the Green's function $G(t,t',x,x')$ is defined as the solution to

$$\mathcal{L}G(t,t',x,x') = \delta(t-t')\delta(x-x'). \tag{2.19}$$

It can be easily checked by substitution that the general solution of the PDE is given by

$$u(t,x) = \int_{-\infty}^{t}\int_{-\infty}^{\infty} G(t,t',x,x')f(t',x')dt'dx'. \tag{2.20}$$

[19] For a dendrite with a radius of 1 μm, we can find typical values of $r_{\mathrm{l}} = 3 \times 10^5 \Omega/\mu\mathrm{m}$, $r_{\mathrm{m}} = 5 \times 10^{11}\Omega\mu\mathrm{m}$ and $c_{\mathrm{m}} = 5 \times 10^{-14}\mathrm{F}/\mu\mathrm{m}$. The corresponding electrotonic length scale and membrane time constant are $\lambda_{\mathrm{m}} = 1.2\,\mathrm{mm}$ and $\tau_{\mathrm{m}} = 25\,\mathrm{ms}$.

In particular, if $\mathcal{L}$ is translation invariant (as it is in our case), G serves as a convolution operator for Eq. 2.20:

$$G(x, x', t, t') = G(x - x', t - t') \tag{2.21}$$

In the following, we will drop all parameters from Eq. 2.13 for clarity. This can be done by rescaling time and space to unit-free coordinates

$$x \to x/\lambda_{\mathrm{m}} \tag{2.22}$$

$$t \to t/\tau_{\mathrm{m}} \tag{2.23}$$

and by additional rescaling of the external current

$$i^{\mathrm{ext}} \to r_{\mathrm{m}} i^{\mathrm{ext}} \tag{2.24}$$

The cable equation then becomes

$$\frac{\partial u}{\partial t} - \frac{\partial^2 u}{\partial x^2} + u = i^{\mathrm{ext}} \tag{2.25}$$

and the Green's function can be given in closed form:

$$G(t, t', x, x') = \frac{\Theta(t - t')}{\sqrt{4\pi(t - t')}} \exp\left[-(t - t') - \frac{(x - x')^2}{4(t - t')}\right]. \tag{2.26}$$

Let us consider a synapse lying at a location that we define as $x = 0$ along a dendrite. Upon arrival of an afferent spike, the current that flows through the synapse and excites the membrane can be modeled as

$$i(t, x) = w^{\mathrm{syn}} \delta(x) \Theta(t) \exp\left[-\frac{t}{\tau^{\mathrm{syn}}}\right]. \tag{2.27}$$

If we neglect boundary effects, we can plug Eqs. 2.27 and 2.26 into Eq. 2.20 to find out how this signal propagates along the dendrite (Fig. 2.15).

As expected, we observe the formation of the characteristic PSP shape at the point of injection (blue curve). The steepness of the rising flank is partly determined by the synaptic time constant τ^{syn}, while the falling flank is largely governed by the membrane time constant τ_{m}. At points lying further away on the dendrite, however, the PSP becomes distorted—the peak voltage is reached later, due to the finite propagation speed of electrical signals along the membrane. Loosely defined as the speed at which the voltage peaks advance, the signal propagation speed is, quite intuitively, a monotonically decreasing function of τ_{m} and a monotonically increasing function of λ_{m}. Additionally, the further away one goes from the point of injection, the smaller the peak voltages become, reflecting the previously discussed effect of the electrotonic length scale.

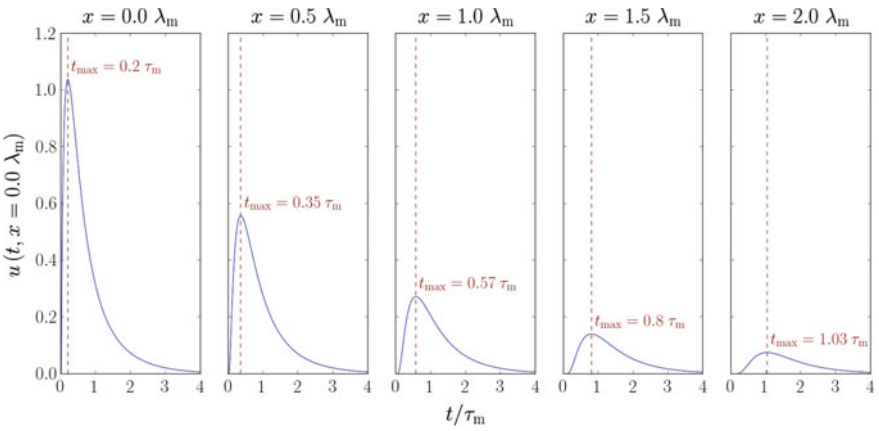

Fig. 2.15 Propagation of membrane potential excitations. The neural cable is excited by a simulated synaptic current with a sudden onset at $t = 0$ and an exponential decay with time constant $\tau^{syn} = \tau_m/5$ at the point $x = 0$ along the membrane. The time course of the membrane potential (PSP) is measured at integer multiples of half the electrotonic length scale $\lambda_m/2$. Two characteristic dispersive effects become apparent. The amplitude of the PSP decreases and it becomes broader as it propagates away from the current injection site. In addition, the rising flank becomes less steep and the peak voltage is reached later, amounting to an effective dendritic delay

We now turn our attention to the propagation of action potentials. By their very nature, it is no longer possible to neglect the active mechanisms that govern their time course. Their propagation is therefore determined by a combination of the passive cable theory from above and the voltage-gated channels from the Hodgkin–Huxley model (Sect. 2.1.2). However, the results we have gained from studying the behavior of purely passive dendrites can give us some important insights.

In order for an AP to propagate from position x further along the axon, it must elicit a high enough voltage change at the position $x + \Delta x$ for the active mechanisms to take over and cause an AP at this new position. The reaction speed to stimuli at any point along the membrane is governed, as we have seen (in e.g. Eq. 2.17 or 2.14), by the membrane time constant τ_m and the electrotonic length scale λ_m. A fast propagation of action potentials towards their target neurons (as would e.g. be required by a quick reaction of the animal to a sensory stimulus) can be aided by two morphological features of axons, both of which have the effect of increasing λ_m.

One straightforward possibility is to increase the diameter of the axon. The total surface area of the axon would grow, allowing more charge to flow through per unit of time, but also requiring more charge per unit of voltage. This would lead to a decrease in r_m but also to a simultaneous increase in c_m, thereby leaving τ_m unaffected. However, the longitudinal resistance r_l would also be reduced, leading to an increase in λ_m and thereby increasing the passive signal propagation speed. Evolution has put this effect to use, as famously illustrated by the millimeter-thick giant squid axons on which Hodgkin and Huxley performed their Nobel-earning experimental work.

However, particularly in younger taxa,[20] evolution has found a more efficient solution. Especially those neurons which require long axonal projections, such as motor neurons which project from the spine to the extremities, have their axons surrounded by a so-called myelin sheath. The myelin is produced by specialized glia called Schwann cells that wrap themselves around the axon in multiple layers, effectively increasing the thickness of the membrane. This decreases the membrane capacitance, but more importantly, it greatly increases the resistance across the membrane. This, in turn, leads to an increase in λ_m and thereby to a faster signal transmission. Between the Schwann cells there remain some unmyelinated axon surface patches, called the nodes of Ranvier. At each such node, the voltage-gated proteins have access to the intercellular medium and can therefore actively "refresh" the AP by the Hodgkin–Huxley mechanism. Due to the "jumping" nature of the APs, their propagation along a myelinated axon is called "saltatory".

The interplay between active and passive transmission also determines the directionality of the AP propagation. Having reached some point along the axon, the AP can not propagate backwards, because those patches of axon membrane lying behind have already been excited and then remain refractory for a significant period of time.

What about the propagation of action potentials from the axon hillock backwards through the dendritic tree? Even without voltage-gated ion channels, APs can still backpropagate by passive transmission only. Moreover, if dendrites are equipped with a high enough density of such channels, the AP propagation should be, in principle, quite similar to the one in unmyelinated axons. Indeed, both varieties of backpropagating APs have been found to occur in nature (Waters et al. 2005). They have been hypothesised to play a significant functional role as well, allowing a sort of feedback mechanism for synaptic plasticity phenomena that require the "knowledge" of both afferent and efferent spiking activity. One such mechanism, called STDP, will be briefly addressed in Sect. 2.2.2.2, where we discuss synaptic plasticity.

We conclude this section with several important remarks. Since spike initiation is quite narrowly localized in space—at the axon hillock—it is both the shape and the timing of the PSPs at that precise site that determines whether the neuron spikes or not. We have seen how these PSP features strongly depend on the position of synaptic current injection, as well as the membrane properties of the dendritic tree (in particular, λ_m and τ_m). We therefore conclude that the morphology of a neural cell is essential to the information processing that it performs. The position of a synapse can, for example, influence both delay-based computation, which is essential in e.g. synfire chain models (see Sect. 5.4), as well as PSP size and shape, which determines functionality in virtually all network models.

As we shall see in the section on simulation software (3.1), dendritic delays can be taken into account for point neuron models, but not morphology-dependent PSP shapes. Modeling the full structure of the dendritic tree would be computationally costly, while also severely limiting the analytical tractability of network dynamics.

[20] It is noteworthy that myelination can also be found in some older taxa as a result of convergent evolution. While not morphologically identical, invertebrate myelin sheaths serve the same functional purpose as in vertebrates.

It is precisely due to their analytic and computational tractability that the remainder of this work is largely dedicated to point neuron models. We therefore need to point out that while the implementation of algorithms in neural networks from a machine learning perspective does not require biological fidelity, any claims about biology coming from single-compartment modeling must be treated with appropriate care and rigor.

2.2 Abstract Models

At this point, we have formulated a mathematical model of biological neuron dynamics and have given an approximate description of synaptic interaction. In its full complexity, our neuron model (Hodgkin–Huxley equations plus the cable equation) is computationally extremely costly, with 4 ODEs for the soma and 1 ODE for each dendritic compartment that is modeled as a single cable (assuming a spike can only be triggered at the soma). Synapse dynamics are even more complicated; modeled in full detail, each synapse would require multiple ODEs for neurotransmitter release at the presynaptic site, diffusion in the synaptic cleft, ligand-gated channeling at the postsynaptic site, neurotransmitter metabolization etc.

If we are to simulate neural networks at the level of individual neurons and synapses, a small set of simple, linear ODEs would be highly advantageous. Simplification, of course, comes at the price of accuracy—or worse, at the expense of functionality, as we have already discussed for the HH model (Sect. 2.1.2). The formulation of abstract models therefore always requires a careful consideration of the tradeoff between functionality (and/or faithfulness to biology) and computational complexity.

In the following, we will elaborate the neuron and synapse models that have been used as building blocks for all the network models discussed in later chapters. Furthermore, these models define the target dynamics of the circuits implemented in our neuromorphic hardware. In Sect. 2.2.1, we will address simplifications of the HH equations and formulate two abstract neuron models: the simple leaky integrate-and-fire model as a stripped-down version of the HH neuron and the more complex adaptive exponential integrate-and-fire model, which even includes dynamics beyond the HH equations. In Sect. 2.2.2, we will formalize synaptic dynamics and discuss two simple models of synaptic plasticity.

2.2.1 Neurons

As already addressed in Sect. 2.1.4, the first simplification we make is to utterly neglect signal propagation in the dendritic tree. We assume our neurons to be point-like, so all input currents have an immediate effect on the membrane potential of the (pointlike) soma. However, the distance of a synapse from the soma, i.e., the

dendritic delay, can still be taken into account. Here, we model the delayed arrival of PSPs at the soma by delaying the arrival of spikes. In both cases, the result is a temporal shift of the PSP incidence at the soma; however, in this model, we lose the (potentially computationally relevant) reshaping of the PSP as a function of the distance it travelled.

In a second step, we reconsider the equations of the HH model, which had been motivated by the desire to have a mechanistic model of the biological dynamics in excitable cells. In particular, most of the model complexity serves almost exclusively for modeling action potentials: the voltage-gated channel dynamics effectively make up three (Eq. 2.6) of the four ODEs—and most of the fourth (Eq. 2.8) as well. However, spikes are generally assumed to be stereotyped events, i.e., with nearly identical shape (Gerstner and Kistler 2002; Dayan and Abbott 2001). Under this assumption, it is only the timing of the individual spikes that matters, thereby rendering its detailed modeling redundant.[21] In many simplified neuron models, the spiking mechanism is therefore replaced by a threshold condition: when a neuron's membrane potential reaches the said threshold at time t_s, it is instantaneously pulled back to a reset value and the neuron "sends a spike" to its efferent neurons. These spikes are typically modeled as a delta function of time. We discuss such a model in Sect. 2.2.1.1.

One needs to remember, however, that the reduction in the number of equations of motion (and the accompanying reduction of the system's phase space spanned by its dynamic variables) invariably leads to a loss of "dynamic richness".[22] In particular, it is impossible to reproduce the driven-oscillator-like subthreshold dynamics of the HH model (see the end of Sect. 2.1.2) in a one-dimensional space. To what extent this results in a loss of computational functionality depends on the network model. In any case, networks based on one-dimensional neuron models can still exhibit extremely interesting dynamics (Chap. 4) and perform complex computational tasks (Chap. 6).

Evidently, the simplified one-dimensional model class outlined above does not need to be the end of the path of abstraction. Indeed, the basic[23] HH model has its own shortcomings and can not capture the entire observed spectrum of single-neuron behavior. This can, however, be remedied by the inclusion of additional dynamic variables which, for example, influence subthreshold dynamics on longer timescales. We shall discuss in detail two network models that rely on 2D neuron dynamics in Chap. 5. Their underlying neuron model is described in detail in Sect. 2.2.1.2.

---

[21] It is important to remember that this, too, is a simplification and does not hold without exception. While most neocortical neurons appear to conform to this assumption, networks exist—e.g., in the elephantnose fish—in which different shapes of action potentials have been measured (Sugawara et al. 1999) and hypothesized to play a functional role (Mohr et al. 2003a, b).

[22] As an example, we mention the Poincaré–Bendixson theorem, which makes a statement about the periodicity of orbits (limit cycles) for two-dimensional dynamical systems. In particular, it forbids the existence of chaotic behavior such as strange attractors. This clearly does not hold for higher-dimensional phase spaces, such as the Lorenz system with its well-known "butterfly attractor".

[23] I.e., with additional dynamics that only cover the generation of action potentials—as described in Sect. 2.1.2 and defined by Eqs. 2.6 and 2.8 with the parameters from Sect. A.1.

2.2.1.1 The Leaky Integrator

The leaky integrate-and-fire (LIF) model is one of the simplest neuron models that can claim biological relevance. It is almost as old as modern neuroscience itself (Lapicque 1907), although its name was introduced only about half a century later (Brunel and Van Rossum 2007). The name basically says it all, and we have already discussed the differential equation of this model in the section on passive membrane properties (Eq. 2.3). A ($\dot{u} \propto -u$)-term represents the leak, whereas the integration of the input current is embedded via $\dot{u} \propto I$:

$$C_\mathrm{m} \frac{du}{dt} = g_\mathrm{l}(E_\mathrm{l} - u) + I^\mathrm{syn} + I^\mathrm{ext}. \tag{2.28}$$

Here, we have subdivided the total input current I into a synaptic component I^syn and a generic external one I^ext. The latter gives additional control over the model and is equivalent to a modulation of E_l. The firing is taken care of by a simple threshold rule: if the membrane potential crosses a threshold ϑ from below,[24] a spike is emitted:

$$\text{neuron spikes at } t = t_\mathrm{spike} \iff u(t_\mathrm{spike}) = \vartheta. \tag{2.29}$$

The outgoing spikes are defined only by the time of their occurrence and form a so-called spike train, which is modeled as

$$\rho(t) = \sum_{\text{spikes } s} \delta(t - t_s). \tag{2.30}$$

Whenever the neuron spikes, its membrane is reset to a potential ϱ. In order to model the refractoriness of biological neurons, the membrane is clamped to the reset potential for a duration τ_ref called the (absolute) refractory time:

$$u(t_\mathrm{spike} < t \leq t_\mathrm{spike} + \tau_\mathrm{ref}) = \varrho. \tag{2.31}$$

The Eqs. 2.28, 2.29 and 2.31 fully define the LIF model. Despite formally being described by three equations, it is important to note that the model itself only has a single dynamic variable, namely the membrane potential u, thus being one-dimensional. It might seem that the synaptic interactions condensed into I^syn offer additional degrees of freedom, but this is not the case, since I^syn is fully determined by the spike trains, and therefore by the membrane potentials, of other neurons in the network—as we shall see in Sect. 2.2.2.

To gain some intuition for this model, we shall briefly describe several simple single-neuron experiments. In particular, this means that there is no synaptic stimulus, so $I^\mathrm{syn} \stackrel{!}{=} 0$. The general solution of the LIF Eq. 2.28 can be easily found:

[24] This is the standard textbook definition, but in this formulation of the model, the "from below" can be omitted, since the equations prevent the membrane potential from ever lying above the threshold.

$$u(t) = u_0 e^{-\frac{t}{\tau_\mathrm{m}}} + \frac{e^{-\frac{t}{\tau_\mathrm{m}}}}{\tau_\mathrm{m}} \int_0^t dt' \left(E_\mathrm{l} + \frac{I^\mathrm{ext}(t')}{g_\mathrm{l}} \right) e^{\frac{t'}{\tau_\mathrm{m}}}. \tag{2.32}$$

If the current remains constant in time, the equation takes an even simpler and more intuitive form:

$$u(t) = E_\mathrm{l} + \frac{I^\mathrm{ext}}{g_\mathrm{l}} + \left(u_o - E_\mathrm{l} - \frac{I^\mathrm{ext}}{g_\mathrm{l}} \right) e^{-\frac{t}{\tau_\mathrm{m}}} \quad , \tag{2.33}$$

where $u_0 := u(t = 0)$ and $\tau_\mathrm{m} = \frac{C_\mathrm{m}}{g_\mathrm{l}}$ represents the membrane time constant (see also Eq. 2.13), which quantifies the relaxation speed of the membrane potential towards the equilibrium value $E_\mathrm{l} + I^\mathrm{ext}/g_\mathrm{l}$ (Fig. 2.16).

If the equilibrium value lies below the spiking threshold ($E_\mathrm{l} + I^\mathrm{ext}/g_\mathrm{l} < \vartheta$), the current stimulus is called subthreshold. The time course of the membrane potential then corresponds to the charging/discharging of a capacitor. If the equilibrium value lies above the spiking threshold ($E_\mathrm{l} + I^\mathrm{ext}/g_\mathrm{l} > \vartheta$), the current stimulus is called suprathreshold. The trajectory of the membrane potential then remains piecewise exponential, but becomes discontinuous, due to the reset when crossing the threshold. Consequently, the LIF neuron fires periodically, with a firing rate that can be computed by setting appropriate boundary conditions for Eq. 2.33:

$$u_0 = \varrho \tag{2.34}$$

$$u(T) = \vartheta \tag{2.35}$$

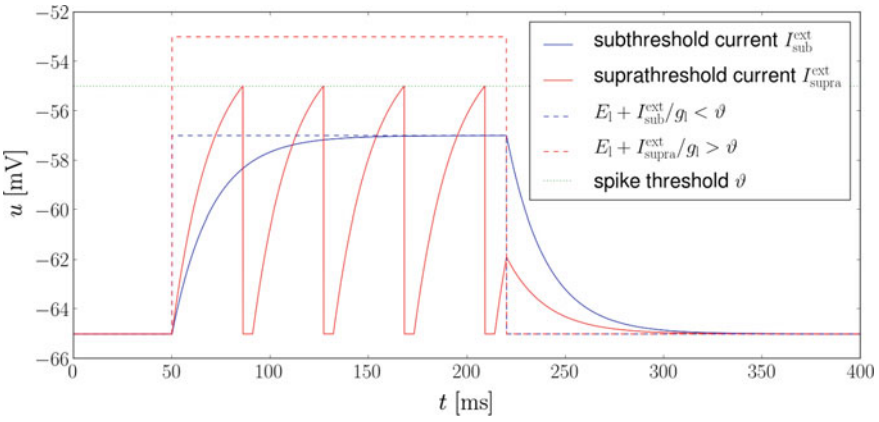

Fig. 2.16 Membrane potential of an LIF neuron with step current stimulus. The membrane potential always converges exponentially towards the equilibrium value $E_\mathrm{l} + I^\mathrm{ext}/g_\mathrm{l}$ with a time constant $\tau_\mathrm{m} = \frac{C_\mathrm{m}}{g_\mathrm{l}}$. During subthreshold stimulation (*blue*), the membrane follows the charge/discharge curve of a capacitor. During suprathreshold stimulation (*red*), the neuron spikes regularly with a rate given by Eq. 2.36

$$\Rightarrow \nu = (\tau_{\text{ref}} + T)^{-1} = \left(\tau_{\text{ref}} + \tau_{\text{m}} \ln \frac{\varrho - E_{\text{l}} - \frac{I^{\text{ext}}}{g_{\text{l}}}}{\vartheta - E_{\text{l}} - \frac{I^{\text{ext}}}{g_{\text{l}}}} \right)^{-1} \tag{2.36}$$

The firing rate of a neuron as a function of its input—in this case, of the input current I^{ext}—is appropriately called an f-I curve. The terms gain function and activation function are often used synonymously in literature. Figure 2.17 shows the f-I curve of two (nearly) identically parametrized LIF neurons, one with and the other without a refractory period.

Without refractoriness, the firing rate diverges for large input currents, as the argument of the logarithm in Eq. 2.36 approaches unity. The asymptotic behavior can be easily found with an appropriate Taylor expansion of Eq. 2.36 in $(I^{\text{ext}})^{-1}$:

$$\nu(I^{\text{ext}}) \overset{I^{\text{ext}} \to \infty}{\approx} \frac{1}{\tau_{\text{m}}(\vartheta - \varrho)} \left(E_{\text{l}} - \frac{\varrho + \vartheta}{2} + \frac{I^{\text{ext}}}{g_{\text{l}}} \right). \tag{2.37}$$

The inclusion of a nonzero refractory period enables a more biologically plausible, convergent behavior towards a finite firing rate which, again, follows directly from Eq. 2.36:

$$\nu(I^{\text{ext}}) \xrightarrow{I^{\text{ext}} \to \infty} \frac{1}{\tau_{\text{ref}}}. \tag{2.38}$$

We shall see the activation function reappear prominently in Chap. 6.

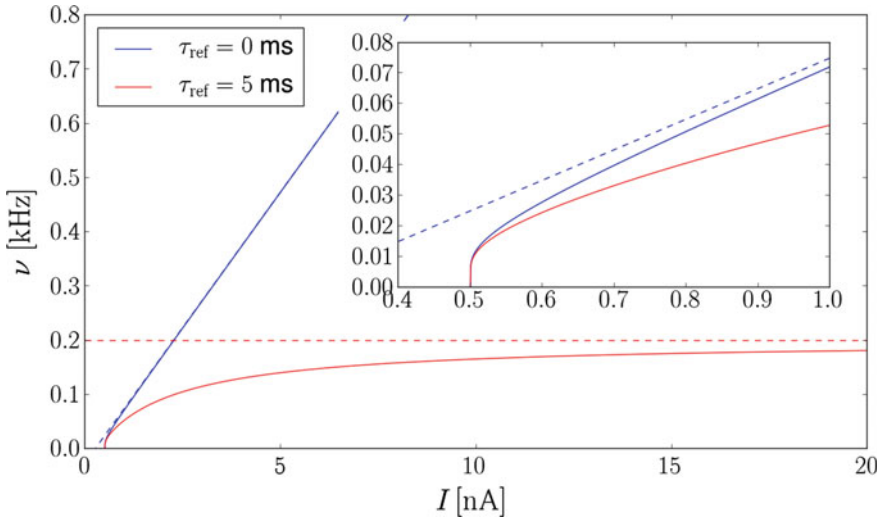

Fig. 2.17 f-I curve of an LIF neuron. Without refractoriness, the firing rate diverges with a linear asymptotic behavior. If the refractory time is nonzero, the firing rate converges towards a maximum value of $1/\tau_{\text{ref}}$. The inset represents a zoom onto the point of firing initiation. We can see that the firing rate is a continuous function of time—there is no jump at $I^{\text{ext}} = 0.5$ nA. This feature is characteristic of type I models

As can be seen in Fig. 2.17, the transition from a non-firing (subthreshold excitation) to a firing state (suprathreshold excitation) is a continuous function of the input current. This is a characteristic feature of so-called type I models, which display a sharp voltage threshold and a zero-frequency onset of stable oscillations (regular spiking). In contrast, so-called type II models do not have a sharp threshold and oscillations start with nonzero frequency. Two examples, both derived as simplifications of the HH model (which is itself of type II), are the Connor model for type I (Connor et al. 1977) and the Fitzhugh–Nagumo model for type II (FitzHugh 1961); depending on their parameters, some models can be either (Morris and Lecar 1981).

It should be noted here that the formal definition of model types varies throughout literature (see,e.g., Ermentrout 1996) and there is no clear-cut criterion for classification. Some authors define the type of the excitability directly from the f-I curve, in which case the LIF model is classified as type I excitable. However, most authors discuss this classification in terms of bifurcation theory (in particular, Hopf vs. saddle-node bifurcations), therefore making it difficult to formally classify the linear LIF model as either type according to these criteria. For a comprehensive discussion of phase plane analysis, we refer to Chap. 3 of Gerstner and Kistler (2002).

2.2.1.2 The Adaptive Exponential Integrate-and-Fire Model

Up to here, we have argued from the perspective that action potentials are stereotyped events with no information contained in their shape but only in their timing. Furthermore, we have implied that the LIF model captures the most important aspects of subthreshold dynamics, rendering any additional terms and equations of the HH model essentially perturbative. We now reconsider these hypotheses by raising two issues.

Let us first consider the spike initiation of an LIF neuron. Due to the firing condition (Eq. 2.29), the spike timing depends critically on the choice of the threshold. Since biological neurons do not have such a threshold, the extraction of this parameter from electrophysiological data is conceivably difficult and prone to error. Even if we loosely define the "biological threshold" as the initiation point of the membrane potential upswing during a spike, then clearly the nonlinear terms in the HH equation play an important role for the membrane dynamics close to this threshold. Such effects can not be captured by a purely linear model such as LIF.

The second argument comes directly from electrophysiological data. A regular oscillatory behavior, as described above for LIF neurons, is only one of many possible responses of different neuron types in the cortex to a constant current stimulus (see,e.g., Markram et al. 2004). In contrast, both the LIF model and the basic HH model can only produce constant-frequency oscillations. The adaptive exponential integrate-and-fire (short: AdEx) model covers both of the above issues—expectably at the price of added complexity.

The issue of spike generation can be addressed by adding nonlinear (current) terms to the equation that governs the membrane potential. In case of the AdEx model, the added term is an exponential function of the membrane potential:

$$I^{\text{exp}} = g_{\text{l}} \Delta_{\text{T}} \exp\left(\frac{u - E_{\text{T}}}{\Delta_{\text{T}}}\right) \tag{2.39}$$

This term offers two degrees of freedom. The threshold voltage E_{T} plays a similar role to the "hard" threshold ϑ in the LIF model. Loosely speaking, when the membrane potential crosses E_{T} from below, I^{exp} begins to dominate the membrane dynamics, pushing the membrane potential even further "upwards". In contrast to the LIF model however, this is not an all-or-none condition: at any point in time, the positive contribution of the exponential term can be countered by an appropriate negative contribution from external stimuli (e.g., inhibitory afferents). The relative strength of I^{exp} is modulated by the so-called slope factor Δ_{T}, which is required to be positive.

The more important issue is the one related to spike pattern complexity. This is addressed by including an additional dynamic variable, the adaptation variable w. It enters the membrane potential ODE linearly and is itself described by a first-order linear ODE with jumps upon spiking. Before we address the resulting dynamics, we first write down the full mathematical description of the AdEx model:

$$C_{\text{m}} \frac{du}{dt} = g_{\text{l}}(E_{\text{l}} - u) + g_{\text{l}} \Delta_{\text{T}} \exp\left(\frac{u - E_{\text{T}}}{\Delta_{\text{T}}}\right) - w + I^{\text{syn}} + I^{\text{ext}} \quad , \tag{2.40}$$

$$\tau_w \frac{dw}{dt} = a(u - E_{\text{l}}) + b\,\tau_w\,\rho - w \quad , \tag{2.41}$$

where $\rho(t)$ represents the neuron's own spike train (Eq. 2.30), and a, b, and τ_w are adaptation parameters discussed below. As these equations still lack a mechanism for pulling down the membrane potential following a spike, the reset mechanism of the LIF neuron is kept in place, albeit with a different, much higher spiking threshold V_{spike}:

$$t_{\text{spike}} \Leftrightarrow u(t_{\text{spike}}) = V_{\text{spike}} \tag{2.42}$$

$$u(t_{\text{spike}} < t \leq t_{\text{spike}} + \tau_{\text{ref}}) = \varrho \tag{2.43}$$

Another advantage of the exponential term becomes apparent here. Barring all constants that can be removed by an appropriate linear transformation of u, the solution to an ODE of type

$$\frac{du}{dt} = \exp(u) \tag{2.44}$$

is

$$u(t) = -\log(c - t). \tag{2.45}$$

Once the exponential term becomes dominant, the membrane potential diverges asymptotically, reaching infinity in finite time (i.e., at $t = c$). Therefore, as long as the cutoff V_{spike} is high enough, the spike timing does not critically depend on the precise choice of V_{spike}.

As mentioned above, the inclusion of a second dynamic variable is the most important departure from the simple LIF model. The time constant τ_w governs the rate at which the adaptation variable w decays back to 0 and is usually on the order of hundreds of ms. The parameter a determines the influence of the membrane potential on the adaptation; it is used to, for example, model variations in the ion concentration caused by sustaining either a high or a low membrane potential. The parameter b represents the quantal increase of the adaptation variable following a spike, sharing a similar electrophysiological motivation as a. Since it only comes into play when the neuron spikes, b is used to emulate so-called spike frequency adaptation (SFA).

Depending on the choice of the parameters a and b, the adaptation variable w can have both an excitatory and an inhibitory effect on the membrane potential. Very often, a and b are chosen to be positive, thereby causing a negative adaptation current and therefore a firing rate that tends to decrease over time. In this case, the adaptation acts as a homeostatic mechanism on both the membrane potential and the spike frequency of the neuron. Figure 2.18 shows an example of adapting AdEx dynamics.

More important, however, is the fact that w enables the AdEx model to emulate a vast array of complex firing patterns, including, but not limited to, the driven oscillations and the inhibitory rebound spiking we discussed earlier for the HH model (Sect. 2.1.2). Figure 2.19 shows an array of typical cortical neuron firing patterns reproduced by an AdEx neuron with appropriate parameter settings. For a much more in-depth discussion of AdEx dynamics, we refer to Gerstner and Brette (2009) and Naud et al. (2008).

On a final note, it should be mentioned that the LIF model is a special case of the AdEx model and can be emulated by an appropriate setting of the parameters Δ_T, a and b. Setting $a = 0$ and $b = 0$ effectively removes adaptation. The exponential term is removed by setting $\Delta_T = 0$, since

$$\lim_{x\to 0, x>0} x \exp(a/x) \overset{y=1/x}{=} \lim_{y\to\infty, y>0} \frac{\exp(ay)}{y} = \begin{cases} 0 & \text{for} \quad a < 0 \\ \infty & \text{for} \quad a > 0 \end{cases} . \tag{2.46}$$

The exponential current then becomes an all-or-none firing condition, rendering E_T formally (and numerically) equivalent to the hard threshold ϑ in the LIF model.[25]

[25] What works well in theory may not be equally unproblematic in practice. Expressions which may converge to finite values, but contain terms that diverge in the required limit, are notoriously problematic in software implementations. Neural simulation software handles such problems with varying degrees of success: NEST 2.1.1, for example, returns an error, while Neuron 7.1 returns

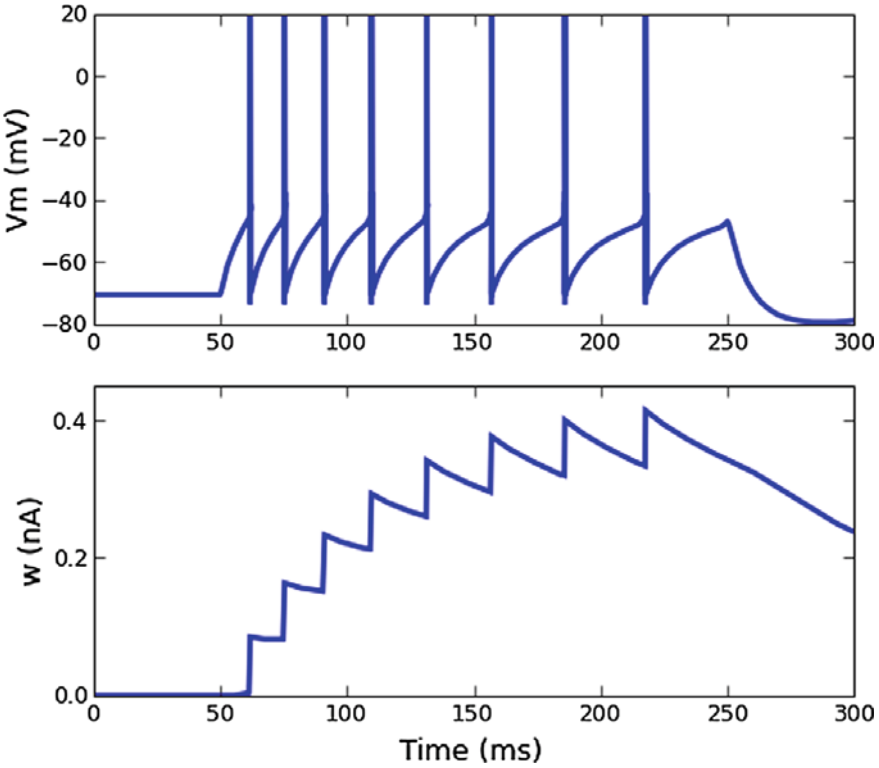

Fig. 2.18 Exemplary dynamics of the AdEx model with a step current stimulus. The parameters were chosen to simulate a slowly adapting behavior (i.e., a slowly decaying firing rate). *Top* temporal evolution of the membrane potential u. The main component of the membrane potential dynamics is the same as in the LIF model: an exponential decay towards an equilibrium potential, as seen in the trace segments that precede the spikes. This equilibrium potential becomes lower over time due to an increasing (negative) adaptation current $-w$. When it exceeds the spike threshold (-50 mV), the membrane potential diverges asymptotically. *Bottom* temporal evolution of the adaptation variable w. The leak component of the adaptation ODE can be easily seen in the exponentially decaying segments between the spikes. The quantal increase following each spike causes the jumps in the trace. The dependence of w on u is a bit more subtle, but it can be seen in the slight increase of w around 50 ms and the inflection point of the curve around 250 ms. Figure taken from Gerstner and Brette (2009)

(Footnote 25 continued)
a warning. Therefore, when such a limit is required (such as for the L23 model fit in Sect. 5.3), particular care needs to be taken. For hardware implementations, such terms become even more problematic, due to limited parameter precision (see Sect. A.2.2). On the HICANN chip, this issue is solved by having the exponential term implemented in a separate circuit that can be effectively decoupled from the cell membrane (see Sect. 3.3.1).

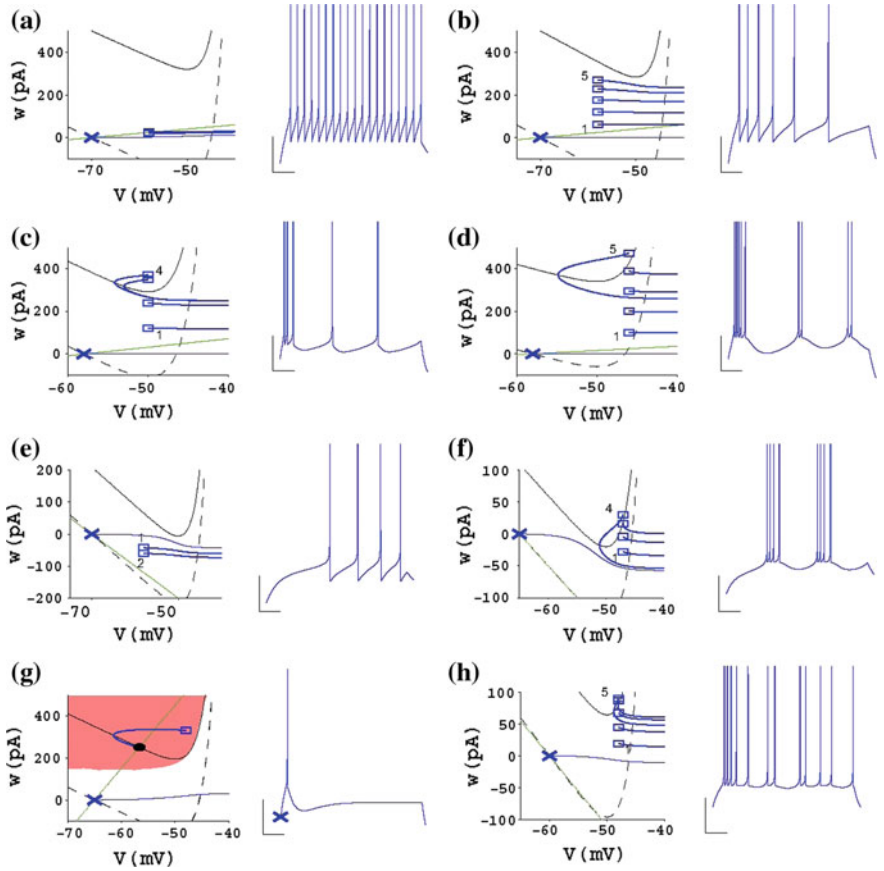

Fig. 2.19 Eight firing patterns generated by AdEx neurons stimulated by a constant current. The voltage traces are shown with scale bars that correspond to 100 ms and 20 mV, respectively. Each of the voltage plots is accompanied by a depiction of the model's trajectories in the phase plane spanned by u and w. (The membrane potential u is denoted by V in the plots.) The locus of states where the temporal derivative of a dynamic variable is zero is called a nullcline. (Therefore, trajectories always cross nullclines either vertically or horizontally.) Intersections between nullclines are called fixed points. As becomes evident from Eqs. 2.41 and 2.40, the w-nullcline (*green*) is a straight line, whereas the u-nullclines (*black*) are a superposition of a linear and an exponential component. The u-nullclines with and without current stimulation are represented as *solid* and *dashed lines*, respectively. The neurons are always initialized at their resting state, i.e. at the (stable) fixed point of the system without current stimulus, which is denoted by a *blue cross*. The reset condition causes the trajectories to be discontinuous: upon spiking, the membrane potential is reset to u_{reset} and the adaptation variable is incremented by b. The points where trajectories reenter the phase plane following a spike are marked by *blue rectangles*. If this happens more than once, the first and last point of reentry are accompanied by the index of the preceding spike. **a** Tonic spiking. **b** Adaptation. **c** Initial burst. **d** Regular bursting. **e** Delayed accelerating. **f** Delayed regular bursting. **g** Transient spiking. The stable fixed point is indicated with a *black*, *filled circle*. **h** Irregular spiking. Figure taken from Naud et al. (2008). The AdEx parameters that were used for the different firing patterns are given in Table 1 of the paper

2.2.2 Synapses

As outlined in Sect. 2.1.3, synaptic interaction is a complex phenomenon, arguably even more complex than the neuron dynamics themselves. For this reason, few, if any, detailed[26] biophysical synaptic models exist. The most widely used synapse models in computational neuroscience are purely phenomenological: synaptic interactions are modeled by stereotypical functions of time called interaction kernels which sum up linearly over space (i.e., over different synapses) and time. The total impact of all synapses can then be written as

$$f^{\mathrm{syn}}(t) = \sum_{\text{synapses } k} \sum_{\text{spikes } s} w_k \epsilon_k (t - t_s) \quad , \tag{2.47}$$

where w_k denotes the weight or strength of the kth synapse and ϵ_k its synaptic interaction kernel. The interaction kernel can, in principle, assume an arbitrary shape, but in most models it is constrained by the biophysics of synaptic interaction. Before addressing the exact nature of the synaptic input f^{syn}, we shall first discuss the shape of the synaptic kernels $\epsilon(t)$.

As described in Sect. 2.1.3, the synaptic release of neurotransmitters happens very quickly, as does their diffusion towards the postsynaptic terminal, due to the narrow width of the synaptic cleft. The removal of neurotransmitters from the postsynaptic terminal, however, may occur on a wide range of time scales, depending on the nature of the transmitter and receptor molecules. Therefore, a useful phenomenological model is the difference-of-exponentials function[27]:

$$\epsilon(t) = A\Theta(t) \frac{1}{\tau_{\mathrm{rise}} - \tau_{\mathrm{fall}}} \left[\exp\left(-\frac{t}{\tau_{\mathrm{rise}}} \right) - \exp\left(-\frac{t}{\tau_{\mathrm{fall}}} \right) \right] \quad , \tag{2.48}$$

where the two exponential functions model the (stochastic) arrival and removal of neurotransmitters at the postsynaptic site, governed by their respective time constants τ_{rise} and τ_{fall}. For now, A simply represents a constant factor that transforms ϵ_k to an amplitude and units of choice.

Very often, even simpler kernels are used in both theoretical and computational approaches. In the limit of identical time constants τ_{rise} and τ_{fall}, the interaction kernel becomes a so-called α-function, as can be easily derived via l'Hôpital's rule:

$$\lim_{\tau_{\mathrm{rise}} \to \tau_{\mathrm{fall}} = \tau^{\mathrm{syn}}} \epsilon(t) \propto \Theta(t) t \exp\left(-\frac{t}{\tau^{\mathrm{syn}}} \right) . \tag{2.49}$$

[26] In the spirit of the Hodgkin–Huxley model of neuron/membrane dynamics.

[27] Incidentally, this function is identical to the PSP shapes derived in Sect. 4.2 (Eqs. 4.39 and 4.59). In order to avoid any confusion, we note explicitly that Eq. 2.48 represents a phenomenological model of *PSCs*, whereas Eqs. 4.39 and 4.59 represents the shape of a *PSP*, i.e., the analytical solution of the LIF equation driven by a single, exponentially shaped PSC.

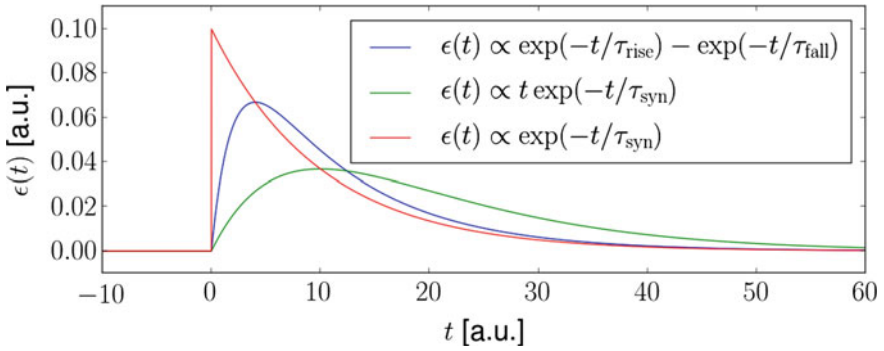

Fig. 2.20 The three different synaptic interaction kernels described in the text. All three kernels have been scaled to unit area. The time constants were set to $\tau_{\text{rise}} = 2$ and $\tau_{\text{fall}} = \tau^{\text{syn}} = 10$ (in arbitrary units of time)

The probably most popular synaptic interaction kernel results from the assumption that the diffusion of neurotransmitters happens much faster than their removal. If one therefore neglects τ_{rise}, the synaptic interaction kernel becomes a simple exponential function:

$$\lim_{\tau_{\text{rise}} << \tau_{\text{fall}} = \tau^{\text{syn}}} \epsilon(t) \propto \Theta(t) \exp\left(-\frac{t}{\tau^{\text{syn}}}\right). \tag{2.50}$$

The three kernels discussed above are depicted in Fig. 2.20. Equation 2.50 represents the synaptic interaction model used from here on throughout this work.

Now that we have established the functional shape of the synaptic interaction, we need to discuss its nature. The neuron model equations discussed in earlier sections (Eqs. 2.28 and 2.40) may suggest that synaptic transmission is equivalent to *current* injection into the membrane. On the other hand, we have explicitly discussed in Sect. 2.1.3 how (chemical) synapses cause an increase in the membrane *conductance* for specific ion types. While the latter is certainly true, arguments can be made for modeling synaptic interactions as currents. Indeed, both current and conductance-based synaptic models are widely used in theoretical and computational neuroscience.[28] Below, we explain the reasoning behind these models and briefly outline their differences. A much more detailed discussion is provided in Sect. 4.2.

2.2.2.1 Current-Based and Conductance-Based Models

Conductance-Based Synaptic Interaction

As outlined in Sect. 2.1.3, an incoming spike causes a synapse to locally change the conductance of the neural membrane towards the reversal potential of the ion type

[28] We point out again that, depending on the context, the abbreviation PSC may refer to either a postsynaptic current or a postsynaptic conductance.

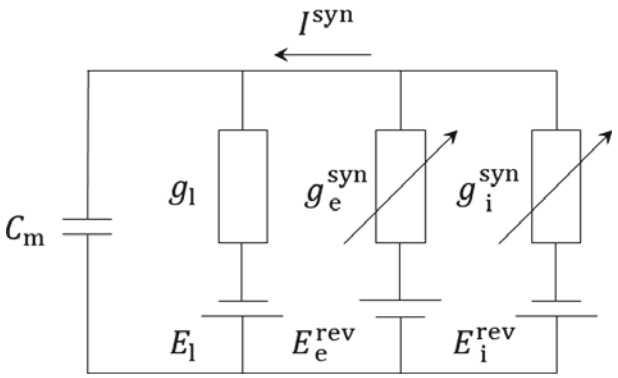

Fig. 2.21 Circuit diagram of an LIF neuron with COBA synapses. Incoming spikes trigger changes in the synaptic conductances towards their respective reversal potential, generating an input current that depends on the momentary value of the membrane potential

its ligand-gated ion channels are permeable for. Consequently, in this scenario, f^{syn} represents a conductance and shall therefore be renamed g^{syn}. Figure 2.21 shows a schematic of the corresponding circuit.

Here, we need to explicitly differentiate between excitatory ($g_{\text{e}}^{\text{syn}}$) and inhibitory ($g_{\text{i}}^{\text{syn}}$) conductances, since they "connect" the membrane to different reversal potentials $E_{\text{e}}^{\text{rev}}$ and $E_{\text{i}}^{\text{rev}}$, respectively. Since membrane dynamics are primarily determined by Na^+ and K^+ flows, the reversal potentials are usually chosen as

$$E_{\text{e}}^{\text{rev}} = E_{\text{Na}^+} \quad \text{and} \tag{2.51}$$

$$E_{\text{i}}^{\text{rev}} = E_{\text{K}^+}. \tag{2.52}$$

We can now apply Ohm's law to the synaptic conductances in Fig. 2.21 to obtain the total synaptic current

$$I^{\text{syn}} = g_{\text{e}}^{\text{syn}}(E_{\text{e}}^{\text{rev}} - u) + g_{\text{i}}^{\text{syn}}(E_{\text{i}}^{\text{rev}} - u). \tag{2.53}$$

This equation underpins the conductance-based (COBA) synaptic model. Note how the synaptic current explicitly depends on the membrane potential. By plugging the synaptic current into the LIF equation (Eq. 2.28), we can now obtain the COBA LIF equation:

$$C_{\text{m}}\frac{du}{dt} = g_{\text{l}}(E_{\text{l}} - u) + g_{\text{e}}^{\text{syn}}(E_{\text{e}}^{\text{rev}} - u) + g_{\text{i}}^{\text{syn}}(E_{\text{i}}^{\text{rev}} - u) + I^{\text{ext}}. \tag{2.54}$$

Despite saving a more thorough discussion for later (Sect. 4.2), we can already point out several important characteristics of the COBA LIF equation. Firstly, the

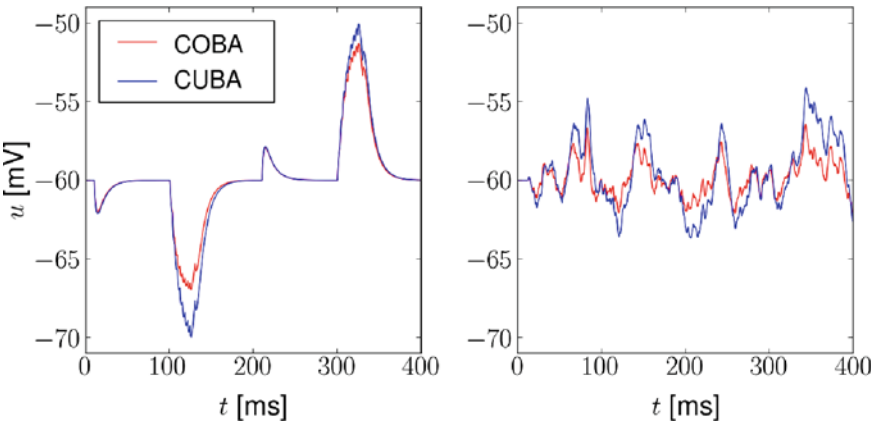

Fig. 2.22 COBA versus CUBA synapses. *Left* PSP saturation as the membrane approaches the inhibitory reversal potential. The effect is visible for excitatory PSPs as well, but is much weaker due to the larger distance towards the excitatory reversal potential. *Right* effect of an increased total conductance. Both the COBA and the CUBA neuron are stimulated with identical excitatory and inhibitory Poisson spike trains. Despite the dynamic range of the membrane potential being smaller than in the *left plot*, the membrane of the CUBA neuron fluctuates significantly stronger than the one of its COBA counterpart. This happens because due to the increased total conductance of the COBA neuron, which leads to a faster membrane and thereby smaller PSPs

relationship between the membrane potential and its derivative is no longer determined only by a constant coupling g_l (as it was in the simple LIF equation), but also by explicit functions of time $g_\mathrm{e}^\mathrm{syn}$ and $g_\mathrm{i}^\mathrm{syn}$. This makes the task of finding a closed-form solution for the temporal evolution of the membrane potential much more difficult (see, in particular, Sect. 4.2.4). Secondly, due to the dependence on the distance towards the reversal potentials, summation of PSPs is no longer linear. This is particularly visible for inhibitory PSPs, where saturation effects can easily appear due to the close proximity of the inhibitory reversal potential to the dynamic range of the membrane potential. This effect is also present, albeit less visible, for excitatory PSPs, in particular since the spike threshold prohibits large depolarizations of the membrane. Thirdly, judging just by the formal equivalence of the three conductance-regulated additive terms in the COBA LIF equation, the total membrane conductance $g^\mathrm{tot} = g_\mathrm{l} + g_\mathrm{e}^\mathrm{syn} + g_\mathrm{i}^\mathrm{syn}$ becomes itself a function of time—and, in particular, larger than g_l alone (since conductances can only be positive by definition). Therefore, the "reaction speed" of the membrane given by its time constant $\tau_\mathrm{eff} = \frac{C_\mathrm{m}}{g^\mathrm{tot}}$ increases and becomes itself time-dependent. This, in turn, causes the effect of an incoming spike on the membrane potential to depend on all other spikes received from all presynaptic partners. Figure 2.22 shows an example of these effects.

By assuming a particular synaptic interaction kernel, we can now provide a closed-form expression for the COBA synapse dynamics. With the exponential kernel from Eq. 2.50, the excitatory and inhibitory synaptic conductances can be written as

$$g_x^{\text{syn}}(t) = \sum_{\text{syn } k} \sum_{\text{spk } s} w_k \Theta(t - t_s) \exp\left(-\frac{t - t_s}{\tau^{\text{syn}}}\right), \quad x \in \{\text{e}, \text{i}\}. \tag{2.55}$$

The total synaptic current I^{syn} then becomes

$$I^{\text{syn}}(t, u) = \sum_{x \in \{\text{e,i}\}} \sum_{\text{syn } k} \sum_{\text{spk } s} w_k \Theta(t - t_s)(E_x^{\text{rev}} - u) \exp\left(-\frac{t - t_s}{\tau^{\text{syn}}}\right). \tag{2.56}$$

Current-Based Synaptic Interaction

While the conductance-based nature of chemical synapses is an empirical fact, it does not necessarily imply that synaptic interaction models must be conductance-based themselves. The reason for this non sequitur lies within the spatial structure of neurons (Sect. 2.1.4). An incoming spike may cause a *local* change in the membrane conductance, but the elicited PSP propagates *passively* towards the soma. The soma therefore only experiences an incoming current and is not affected by distal conductance dynamics. If one wishes to use a point neuron model, it is somewhat natural to consider the "point" to represent the soma, since it is there where the afferent inputs are summed up to generate action potentials. It can therefore be argued that a current-based (CUBA) synaptic interaction model is more natural when combined with a point neuron model.

In this scenario, the membrane potential equation remains identical to Eq. 2.28:

$$C_{\text{m}} \frac{du}{dt} = g_{\text{l}}(E_{\text{l}} - u) + I^{\text{syn}} + I^{\text{ext}}. \tag{2.57}$$

With the exponential kernel from Eq. 2.50, the total synaptic current can be written as

$$I^{\text{syn}}(t) = \sum_{\text{syn } k} \sum_{\text{spk } s} w_k \Theta(t - t_s) \exp\left(-\frac{t - t_s}{\tau^{\text{syn}}}\right) \tag{2.58}$$

These equations express the fact that, in contrast to the COBA scenario, CUBA PSPs are summed up linearly and do not otherwise interact with each other. As we shall see in Sect. 4.2, this greatly simplifies the analytical treatment of membrane potential dynamics.

We end this section with a brief explanation of commonly used nomenclature for the synapse dynamics discussed above. Network models in computational neuroscience rarely use different types of neuron or synapse models simultaneously. Furthermore, any single neuron usually has the same dynamics for all of its afferent synapses. As a consequence, synaptic attributes are often allocated to the used neuron model. Therefore, it is common to speak of, e.g., "COBA EXP LIF neurons",[29]

[29] In PyNN, for example, neuron models implicitly characterize their synapse dynamics. This is accounted for by the typical naming of neuron models, such as, e.g., `IF_cond_alpha` or `aEIF_curr_exp`.

despite the fact that COBA EXP characterizes the synapse model and LIF the neuron membrane dynamics.

2.2.2.2 Synaptic Plasticity

In living tissue, the coupling strength between neurons is not a fixed quantity, but may change over time. These variations can be tracked back to morphological changes in their synaptic connections. which can be broadly classified based on the time scales on which they occur. In this section, we will only give a brief overview of theoretical models of synaptic plasticity. In particular, short-term plasticity will play an important role in the dynamics of the spiking network models discussed in Sects. 5.3 and 6.5. For a more detailed discussion of synaptic plasticity, we recommend "Part three" (Chaps. 10–12) of the textbook by Gerstner and Kistler (2002) and "Part III" (Chaps. 8–10) of the textbook by Dayan and Abbott (2001).

Structural Plasticity

On very long time scales in the order of days to years, neurons in the brain rewire as a consequence of, e.g., cognitive (learning, memory formation), genetic (aging) or environmental (injury, disease) factors. The formation of new connections and pruning of old ones is called structural plasticity and is mediated by highly complex biochemistry: it involves not only electrical interactions, but also multiple molecular signalling pathways (neurotransmitters, genetic factors etc.). While providing a fertile ground for modern experimental techniques (Caroni et al. 2012), the complex nature of structural plasticity has so far forestalled the formulation of a unified theory, making it a rare sight in computational and theoretical neuroscience models.

Long-Term Plasticity: Rate-Based Models

On intermediate time scales in the order of minutes to hours, existing synapses may also change their weight. Depending on whether synapses are strengthened or weakened, one speaks of long-term potentiation (LTP) and long-term depression (LTD), respectively.[30] A well-known rule of thumb for LTP was coined by Donald O. Hebb (2002): "When an axon of cell A is near enough to excite cell B and repeatedly or persistently takes part in firing it, some growth process or metabolic change takes place in one or both cells such that A's efficiency, as one of the cells firing B, is increased."—which is often paraphrased as "What fires together wires together." This is commonly referred to as Hebb's law and has found its way in many models of synaptic plasticity.

[30] Sometimes long-term and short-term plasticity are abbreviated as LTP and STP, respectively. This can be easily confused with long-term and short-term potentiation and must be inferred from the context, if necessary. Here, we use "P" as an abbreviation for potentiation and do not abbreviate short-term- and long-term plasticity.

Most mathematical formulations of Hebbian learning rules are rate-based and can generally be written as

$$\frac{dw_{ij}}{dt} = F(w_{ij}, \nu_i, \nu_j) \quad , \tag{2.59}$$

where w_{ij} denotes the synaptic weight between the presynaptic neuron j and the postsynaptic neuron i and ν_j and ν_i their respective firing rates. In order to account for Hebb's law, the function F usually features a positive dependence on the product of the neurons' firing rates. In the rare cases where the dependence is chosen to be negative, the plasticity rule is called anti-Hebbian.

The simplest possible rate-based Hebbian learning rule is given by

$$\frac{dw_{ij}}{dt} = c\nu_i\nu_j. \tag{2.60}$$

For positive c—which conforms to Hebb's law—synapses are strengthened when both the pre- and postsynaptic neuron fire. This is also an obvious drawback of this simple model: synaptic weights increase indefinitely for nonzero firing rates. However, this can be easily fixed by introducing an upper bound to the learning rate c:

$$c \to c(w_{ij}) = \gamma(w^{\max} - w_{ij})^{\beta}. \tag{2.61}$$

Still, this model has the limitation that it can not simultaneously account for LTP and LTD (and neither does Hebb's original rule). This can, however, be included, by allowing more complex functions F, along with more complex behavior with various functional consequences. Below, we list three such learning rules that have enjoyed relative popularity in theoretical studies.

The so-called covariance rule proposed in Sejnowski (1977) strengthens the synapse if neural activity is positively correlated and weakens it otherwise:

$$\frac{dw_{ij}}{dt} = \gamma(\nu_i - \langle\nu_i\rangle)\left(\nu_j - \langle\nu_j\rangle\right). \tag{2.62}$$

By adding a quadratic term to the plasticity equation, Oja's rule

$$\frac{dw_{ij}}{dt} = \gamma(\nu_i\nu_j - w_{ij}\nu_i^2) \tag{2.63}$$

enables a homeostatic mechanism of sorts: under certain conditions, it can be shown that the afferent weights of a neuron converge asymptotically to a configuration where $\sum_j w_{ij}^2 = 1$ (Oja 1982). Finally, the plasticity rule proposed by Bienenstock, Cooper and Munro (BCM rule, see Fig. 2.23)

$$\frac{dw_{ij}}{dt} = c_1\nu_i^2\nu_j - c_2\nu_i\nu_j \tag{2.64}$$

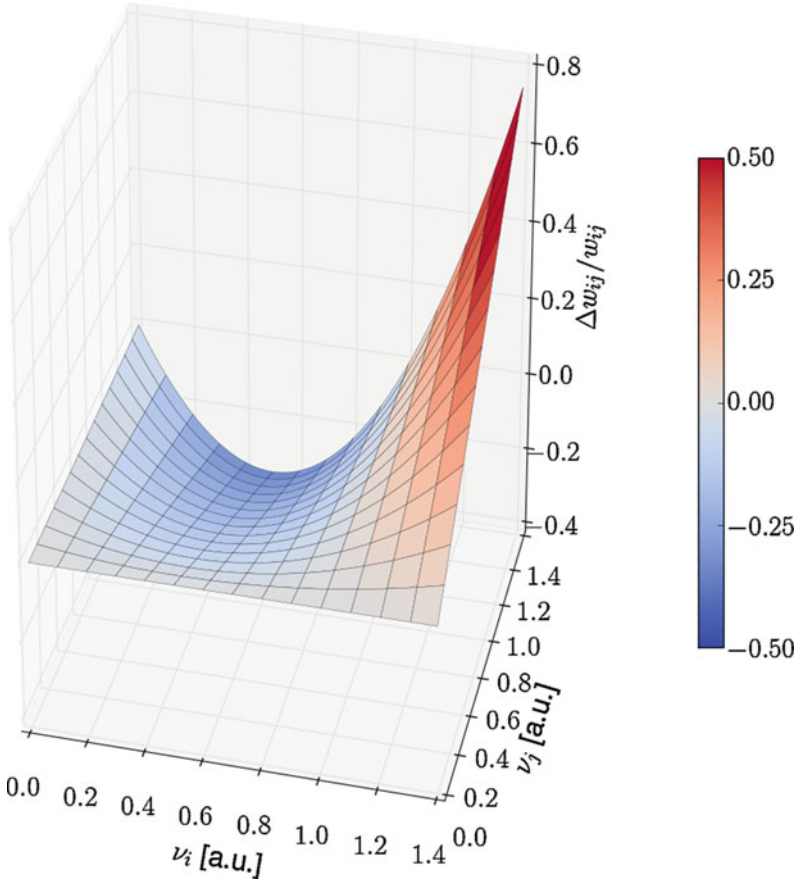

Fig. 2.23 BCM plasticity rule. The parameters c_1 and c_2 in Eq. 2.64 were both set to 1. Depending on the postsynaptic firing rate ν_i, the synapse is either weakened (LTD, *blue hue*) or strengthened (LTP, *red hue*). The fixed point defined by $\frac{\Delta w_{ij}}{w_{ij}} \stackrel{!}{=} 0$ is unstable. The presynaptic firing rate ν_j serves as a linear modulator of the change in synaptic strength

allows neurons to become selective to particular input patterns and has been successfully used to model the development of receptive fields (Bienenstock et al. 1982).

Long-Term Plasticity: Spike-Based Models

The above considerations are based on empirical observation and successfully reproduce some experimentally verified phenomena, but remain at a rather abstract level. In particular, they make no statement about how firing rates are encoded at the site of a particular synapse and offer no mechanistic model of how an individual synapse performs the required computation of $F(w_{ij}, \nu_i, \nu_j)$. For a better understanding of

the microscopic phenomena that enable long-term plasticity, having a spike-based plasticity rule is more convenient.

The arguably most popular spike-based model is STDP, which is short for spike-timing-dependent plasticity. It is based on the observation that the timing of pre- and postsynaptic spikes is critical to the evolution of synaptic weights (Markram et al. 1997; Bi and Poo 1998). While by now a lot of experimental evidence for STDP exists, Fig. 2.24 probably remains the most recognizable result of an STDP measurement protocol. Given these measurements, it is quite straightforward to formulate a phenomenological STDP model.

For any pair of pre- and postsynaptic spikes, we can define the synaptic weight change to be some function W of the difference in spike timing, as well as of the current synaptic weight itself. For any pre- and postsynaptic spike trains ρ_j and ρ_i (as defined in Eq. 2.30), the total synaptic weight change can be written as a sum over all weight changes induced by all pre- and postsynaptic spike pairings:

$$\Delta w_{ij} = \sum_{\text{postsynaptic spikes } k} \sum_{\text{presynaptic spikes } l} W(w_{ij}, t_i^k - t_j^l). \tag{2.65}$$

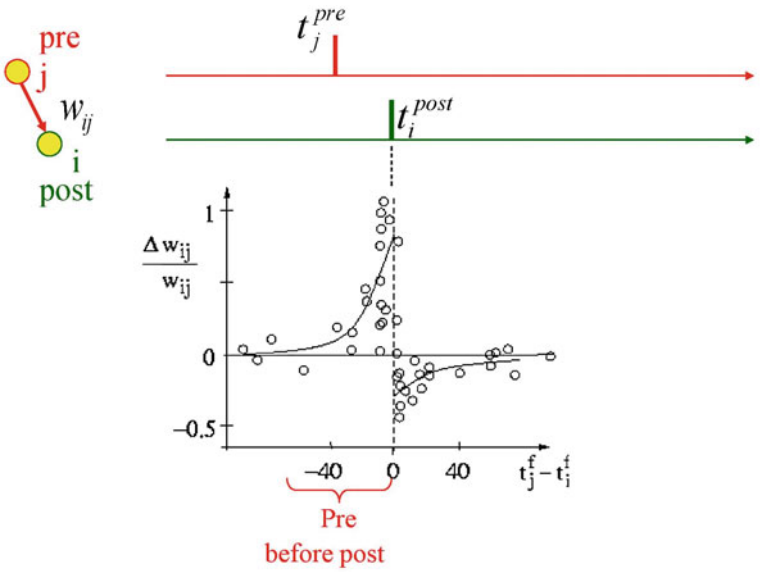

Fig. 2.24 In-vitro measurement of STDP for an excitatory synapse. The *black circles* denote individual measurements of the EPSP amplitude, which reflects the synaptic weight. When the presynaptic neuron spikes before the postsynaptic one (causal relation), the synapse is strengthened. When the timing of pre- and postsynaptic spikes is reversed (acausal relation), the synapse is weakened. The relative weight change is largest when the pre- and postsynaptic spikes appear in quick succession, regardless of their order. The overlayed *solid line* represents a schematic timing-dependent learning rule $W(t_i, t_j)$. Figure taken from Sjöström and Gerstner (2010), which is itself modified from Bi and Poo (1998)

The function W is generally split, depending on the relative timing of the pre- and postsynaptic neuron $\Delta t := t_i^k - t_j^l$, into a causal and an acausal branch:

$$W(w_{ij}, \Delta t) = \begin{cases} A_+(w_{ij}) \exp\left(-\frac{\Delta t}{\tau_+}\right) & \text{for} \quad \Delta t > 0 \quad \text{(causal branch)} \\ -A_-(w_{ij}) \exp\left(\frac{\Delta t}{\tau_-}\right) & \text{for} \quad \Delta t < 0 \quad \text{(acausal branch).} \end{cases} \tag{2.66}$$

The causal and acausal branches are also often called Hebbian and anti-Hebbian, respectively. In most models, the function W factorizes into a pure weight-dependent term A and a pure spike-timing-dependent term. For simplicity and analytical tractability, the latter is often chosen as a decaying exponential function of the pre- and postsynaptic spike interval, which is also in reasonable agreement with the experimental data shown in Fig. 2.24.

In this formulation, the weight-dependent term can be chosen individually for each branch ("+" encodes the causal and "−" the acausal branch):

$$A_+(w_{ij}) = f(w^{\max} - w_{ij})\eta_+ \quad \text{and} \tag{2.67}$$

$$A_-(w_{ij}) = f(w_{ij} - w_{\min})\eta_-. \tag{2.68}$$

The parameters η_+ and η_- represent learning rates. For reasons of physical plausibility, the synaptic weights are bounded from above and below by $w^{\max}$ and $w_{\min}$, respectively. The function f controls the shape of the weight dependence. Popular choices include the soft-bounded multiplicative update rule

$$f(x) = x \tag{2.69}$$

and the additive rule with hard bounds

$$f(x) = \Theta(x) \quad , \tag{2.70}$$

where Θ denotes the Heaviside step function.

In order to avoid a switch from excitation to inhibition, it is usually assumed that $w_{\min} \geq 0$. Apart from being theoretically problematic, such a switch would cause a violation of Dale's law (see Sect. 2.1.3); in particular, it would be biologically implausible, since excitation and inhibition are usually mediated by different neurotransmitters. Indeed, the existence of "inhibitory STDP" has not yet been properly studied.

As already mentioned, the STDP model described here, while very popular with computational and theoretical neuroscientists, remains purely phenomenological. However, it is significantly closer to an electrophysiological explanation of long-term plasticity than the rate-based models described in the previous section. In this model, the synapse only needs to "know" the timing of pre- and postsynaptic spikes. While the former is trivial, the latter has been shown to be possible by action potentials that

propagate back from the soma throughout the dendritic tree (Markram and Sakmann 1995). While the biological basis of STDP is not yet completely understood, the standard STDP model described above has evolved into more complex STDP models based on experimentally established synaptic molecular dynamics (see,e.g., Shouval et al. 2010). Moreover, these models also typically strive to explain the vast array of different STDP shapes observed across different species and brain regions (Abbott and Nelson 2000).

Short-Term Plasticity: The Tsodyks–Markram Mechanism

Changes in synaptic efficacies also occur on shorter timescales, on the order of milliseconds to seconds. Such changes are usually due to physiological reasons and do not necessarily encode learning processes, since they are only transient. However, since they are practically ubiquitous in neural tissue (see, e.g., Thomson and Deuchars 1994), they do play an important role in the way the brain encodes and processes information.

Many experiments have demonstrated that synaptic efficacy is influenced by the firing rate of the presynaptic neuron. Both weakening and strengthening of synapses have been observed, sometimes even simultaneously (see,e.g. Markram et al. 1998a for an extensive collection of experimental papers). Analogously to their long-term counterparts, these short-term synaptic weight changes are abbreviated as STD (short-term depression) and STP (short-term potentiation). Here, we discuss a phenomenological model of short-term synaptic plasticity: the Tsodyks–Markram-Model (short: TSO, see Tsodyks and Markram 1997). For a comprehensive list of biophysical models, we again refer to the review by Markram et al. (1998a).

Initially, the TSO model was designed for representing STD only and was extended later to encompass STP as well. We shall therefore also start with a discussion of STD in the TSO model. The TSO model assumes that the total amount of synaptic resources, which could, for example, model the total number of vesicles within a synapse, is naturally limited and subdivided into three partitions: recovered, effective and inactive, which assume the fractions R, E and I of the total resource amount, respectively. The first model equation must therefore read

$$R + E + I = 1. \tag{2.71}$$

When the synapse is not activated by presynaptic spikes, all resources are collected into the recovered partition, such that the resting state is $(R, E, I) = (1, 0, 0)$. Upon arrival of a presynaptic spike, a portion U (utilization of synaptic efficacy) of the recovered partition is instantaneously transferred to the effective partition, which can be interpreted as neurotransmitter release into the synaptic cleft. The net synaptic effect (postsynaptic current/conductance) is therefore considered proportional to the amount of resources in the effective partition. The effective partition inactivates exponentially with a time constant τ_{inact}, which models the removal of neurotransmitters from the postsynaptic site and is therefore equivalent to the synaptic time constant τ^{syn} from Eq. 2.50. The resources removed from the effective partition are

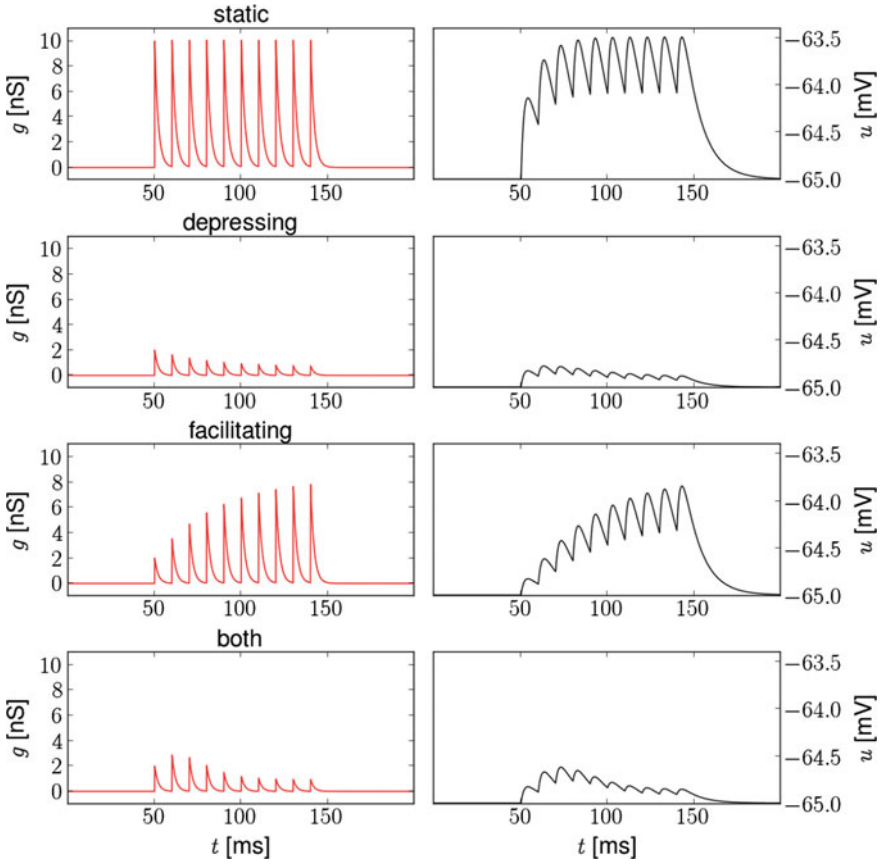

Fig. 2.25 Simulation of synaptic plasticity using the TSO mechanism. The cell is stimulated by a 100 Hz regular spike train for 100 ms. Synaptic efficacy is plotted on the *left* hand side and the resulting membrane potential trace on the *right* hand side. U_0 was set to 0.2, so the first PSC/PSP in the topmost example (no TSO) is five times as high as the first PSCs/PSPs of the other three examples. The synaptic time constant (equivalent to τ_{inact}) was set to 2 ms. For the purely depressing mode, we have set $\tau_{\text{rec}} = 100\,\text{ms}$ and $\tau_{\text{facil}} = 0\,\text{ms}$. For the purely facilitating mode, we have set $\tau_{\text{rec}} = 0\,\text{ms}$ and $\tau_{\text{facil}} = 200\,\text{ms}$. The third mode is a combination of the previous two, with $\tau_{\text{rec}} = 100\,\text{ms}$ and $\tau_{\text{facil}} = 200\,\text{ms}$. Note how in this regime, where STD and STP are happening simultaneously, the synaptic efficacy first rises before dropping off

transferred to the inactive partition, which then decays exponentially back into the recovered partition with a recovery time constant τ_{rec}, thereby modeling neurotransmitter reuptake by the presynaptic terminal. With this, the TSO model of STD is fully defined and we can cast its dynamics into equations:

$$\frac{dR}{dt} = \frac{I}{\tau_{\text{rec}}} - \sum_{\text{spikes } s} UR\,\delta(t - t_s) \tag{2.72}$$

$$\frac{dE}{dt} = -\frac{E}{\tau_{\text{inact}}} + \sum_{\text{spikes } s} UR\,\delta(t - t_s) \tag{2.73}$$

Note that the dynamics of I must not be explicitly given, since they follow directly from Eqs. 2.71–2.73.

In order to model STP, the original TSO model from Tsodyks and Markram (1997) was extended in Markram et al. (1998b) by making U itself a dynamic variable. The first incoming spike of a train triggers a resource transfer of amplitude U_0, but with each incoming spike, U is increased by a certain amount ΔU. By setting $\Delta U = U_0(1 - U)$, one can ensure that the synapse may never use more resources than it has available. In between spikes, U decays back towards its resting state U_0 with a facilitation time constant τ_{facil}. The final equation of the complete TSO model thereby reads:

$$\frac{dU}{dt} = \frac{U_0 - U}{\tau_{\text{facil}}} + \sum_{\text{spikes } s} U_0(1 - U)\ \delta(t - t_s) \tag{2.74}$$

Typically, synaptic time constants are much shorter than those of short-term plasticity (both depression and facilitation). By integrating Eqs. 2.72–2.74 under this assumption, we can calculate the change in the TSO variables as a function of the interspike interval Δt:

$$R_{n+1} = R_n(1 - U_{n+1}) \exp\left(\frac{-\Delta t}{\tau_{\text{rec}}}\right) + 1 - \exp\left(\frac{-\Delta t}{\tau_{\text{rec}}}\right) \tag{2.75}$$

$$E_{n+1} = E_n \exp\left(\frac{-\Delta t}{\tau_{\text{inact}}}\right) + R_n U_{n+1} \exp\left(\frac{-\Delta t}{\tau_{\text{inact}}}\right) \tag{2.76}$$

$$U_{n+1} = U_n \exp\left(\frac{-\Delta t}{\tau_{\text{facil}}}\right) + U_0\left[1 - U_n \exp\left(\frac{-\Delta t}{\tau_{\text{facil}}}\right)\right]. \tag{2.77}$$

For a constant presynaptic firing frequency ν, we can now easily derive steady-state expressions for the TSO variables by setting $X_{n+1} \stackrel{!}{=} X_n =: \tilde{X}$ (with $X \in R, E, U$):

$$\tilde{U} = \frac{U_0}{1 - (1 - U_0)\exp\left(-\frac{1}{\nu\tau_{\text{facil}}}\right)} \tag{2.78}$$

$$\tilde{R} = \frac{1 - \exp\left(-\frac{1}{\nu\tau_{\text{rec}}}\right)}{1 - (1 - \tilde{U})\exp\left(-\frac{1}{\nu\tau_{\text{rec}}}\right)} \tag{2.79}$$

$$\tilde{E} = \frac{\tilde{R}\tilde{U}\exp\left(-\frac{1}{\nu\tau_{\text{inact}}}\right)}{1 - \exp\left(-\frac{1}{\nu\tau_{\text{inact}}}\right)}. \tag{2.80}$$

Figure 2.25 shows several examples of STD, STP and a combination of both using the TSO mechanism.

The TSO mechanism of short-term plasticity plays an important role in later sections of this manuscript. In the cortical attractor memory model discussed in Sect. 5.3, it takes part in controlling the duration of particular activity patterns. In the LIF-based sampling networks from Sect. 6.5, it is used to constrain interneuron coupling strengths by simulating renewing synapses.

References

L.F. Abbott, S.B. Nelson, Synaptic plasticity: taming the beast. Nature Neurosci. **3**, 1178–1183 (2000)

B. Alberts, D. Bray, J. Lewis, M. Raff, K. Roberts, J.D. Watsonx, *Molecular Biology of the Cell*, 3rd edn. (Garland Publishing Inc, New York 1994) ISBN 0815316208

J. Ambros-Ingerson, W.R. Holmes, Analysis and comparison of morphological reconstructions of hippocampal field ca1 pyramidal cells. Hippocampus **15**, 302–315 (2005)

G.Q. Bi, M.M. Poo, Synaptic modifications in cultured hippocampal neurons: dependence on spike timing, synaptic strength, and postsynaptic cell type. J. Neurosci.: Off. J. Soc. Neurosci. **18**(24), 10464–10472 (1998). http://www.jneurosci.org/content/18/24/10464.abstract. ISSN 0270-6474

E.L. Bienenstock, L.N. Cooper, P.W. Munro, Theory for the development of neuron selectivity: orientation specificity and binocular interaction in visual cortex. J. Neurosci. **2**(2), 32–48 (1982)

N. Brunel, M.C. Van Rossum, Lapicque's 1907 paper: from frogs to integrate-and-fire. Biol. Cybern. **97**(5–6), 337–339 (2007)

P. Caroni, F. Donato, D. Muller, Structural plasticity upon learning: regulation and functions. Nature Rev. Neurosci. **13**(7), 478–490 (2012)

J.A. Connor, D. Walter, R. McKowN, Neural repetitive firing: modifications of the Hodgkin–Huxley axon suggested by experimental results from crustacean axons. Biophys. J. **18**(1), 81 (1977)

P. Dayan, L.F. Abbott, *Theoretical Neuroscience: Computational and Mathematical Modeling of Neural Systems* (MIT press, Cambride, Massachusetts, 2001)

J.C. Eccles, From electrical to chemical transmission in the central nervous system. Notes Rec. R. Soc. Lond. 1 **30**(2), 219–230 (1976)

J.C. Eccles, P. Fatt, K. Koketsu, Cholinergic and inhibitory synapses in a pathway from motor-axon collaterals to motoneurones. J. Physiol. **126**, 524–562 (1954)

B. Ermentrout, Type i membranes, phase resetting curves, and synchrony. Neural Comput. **8**(5), 979–1001 (1996)

R. FitzHugh, Impulses and physiological states in theoretical models of nerve membrane. Biophys. J. **1**(6), 445–466 (1961)

W. Gerstner, R. Brette, Adaptive exponential integrate-and-fire model. Scholarpedia **4**(6), 8427 (2009). doi:10.4249/scholarpedia.8427. http://www.scholarpedia.org/article/Adaptive_exponential_integrate-and-fire_model

W. Gerstner, W. Kistler, *Spiking Neuron Models: Single Neurons, Populations* (Cambridge University Press, Cambridge, 2002). Plasticity

C.G. Gross, Aristotle on the brain. Neuroscientist **1**(4), 245–250 (1995)

D. Hebb, *The Organization of Behavior: A Neuropsychological Theory*, (Taylor & Francis, Abingdon, 2002) ISBN 9780805843002

A.L. Hodgkin, The croonian lecture: Ionic movements and electrical activity in giant nerve fibres. Proc. R. Soc. B **148**(930), 1–37 (1958)

A.L. Hodgkin, A.F. Huxley, A quantitative description of membrane current and its application to conduction and excitation in nerve. J. Physiol. 117(4), 500–544, (1952). http://view.ncbi.nlm.nih.gov/pubmed/12991237. ISSN 0022-3751

E.M. Izhikevich, *Dynamical Systems in Neuroscience* (MIT Press, Cambridge, 2007)

W. Kistler, W. Gerstner, J.L. van Hemmen, Reduction of the Hodgkin–Huxley equations to a single-variable threshold model. Neural Comput. **9**, 1015–1045 (1997)

H. Knodel, *Linder Biologie* (Schroeder, Hannover, 1998)

H.T. Kurata, D. Fedida, A structural interpretation of voltage-gated potassium channel inactivation. Prog. Biophys. Mol. Biol. **92**(2), 185–208 (2006). http://dx.doi.org/10.1016/j.pbiomolbio.2005.10.001. http://www.sciencedirect.com/science/article/pii/S0079610705000635. ISSN 0079-6107

N. Lane, W.F. Martin, The energetics of genome complexity. Nature **467**, 929–934 (2010)

N. Lane, W.F. Martin, The origin of membrane bioenergetics. Cell **151**(7), 1406–1416 (2012)

L. Lapicque, Recherches quantitatives sur l'excitation electrique des nerfs traitee comme une polarization. Journal de Physiologie et Pathologie General **9**, 620–635 (1907)

S.B. Long, X. Tao, E.B. Campbell, R. MacKinnon, Atomic structure of a voltage-dependent k+ channel in a lipid membrane-like environment. Nature **450**, 276–382 (2007)

H. Markram, B. Sakmann, Action potentials propagating back into dendrites trigger changes in efficacy of single-axon synapses between layer v pyramidal neurons. Soc. Neurosci. Abstr. **21**, 2007 (1995)

H. Markram, J. Lübke, M. Frotscher, B. Sakmann, Regulation of synaptic efficacy by coincidence of postsynaptic aps. Science **275**, 213–215 (1997)

H. Markram, A. Gupta, A. Uziel, Y. Wang, M. Tsodyks, Information processing with frequency-dependent synaptic connections. Neurobiol. Learn Mem. **70**(1–2), 101–112 (1998a)

H. Markram, Y. Wang, M. Tsodyks, Differential signaling via the same axon of neocortical pyramidal neurons. Proc. Natl. Acad. Sci. USA **95**(9), 5323–5328 (1998b). http://view.ncbi.nlm.nih.gov/pubmed/9560274. ISSN 0027-8424

H. Markram, M. Toledo-Rodriguez, Y. Wang, A. Gupta, G. Silberberg, C. Wu, Interneurons of the neocortical inhibitory system. Nature Rev. Neurosci. **5**(10), 793–807 (2004)

C. Mohr, P.D. Roberts, C.C. Bell, The mormyromast region of the mormyrid electrosensory lobe. i. responses to corollary discharge and electrosensory stimuli. J. Neurophysiol. **90**(2), 1193–1210 (2003a)

C. Mohr, P.D. Roberts, C.C. Bell, The mormyromast region of the mormyrid electrosensory lobe. ii. responses to input from central sources. J. Neurophysiol. **90**(2), 1211–1223 (2003b)

C. Morris, H. Lecar, Voltage oscillations in the barnacle giant muscle fiber. Biophys. J. **35**(1), 193–213 (1981)

R. Naud, N. Marcille, C. Clopath, W. Gerstner, Firing patterns in the adaptive exponential integrate-and-fire model. Biol. Cybern. **99**(4), 335–347 (2008). doi:10.1007/s00422-008-0264-7. http://dx.doi.org/10.1007/s00422-008-0264-7

E. Oja, A simplified neuron model as a principal component analyzer. J. Math. Biol. **15**, 267–273 (1982)

W.F. Pickard, Generalizations of the Goldman–Hodgkin–Katz equation. Math. Biosci. **30**(1), 99–111 (1976)

D. Purves, A.G.J. Horrevoets, F.D. Huijzendveld, *Neuroscience*. Sinauer Associates (2001)

S.G. Schultz, T.E. Andreoli, A.M. Brown, D.M. Farmbrough, J.F. Hoffman, M.G. Welsh, *Molecular Biology of Membrane Transport Disorders* (Plenum Press, New York, 1996)

T.J. Sejnowski, Storing covariance with nonlinearly interacting neurons. J. Math. Biol. **69**, 385–389 (1977)

H.Z. Shouval, S.S.-H. Wang, G.M. Wittenberg, Spike timing dependent plasticity: a consequence of more fundamental learning rules. Front. Comput. Neurosci. **4**, (2010)

J. Sjöström, W. Gerstner, Spike-timing dependent plasticity. Scholarpedia **5**(2), 1362 (2010). doi:10.4249/scholarpedia.1362. http://www.scholarpedia.org/article/Spike-timing_dependent_plasticity

Y. Sugawara, K. Grant, V. Han, C.C. Bell, Physiology of electrosensory lateral line lobe neurons in gnathonemus petersii. J. Exp. Biol. **202**(10), 1301–1309 (1999)

A.M. Thomson, J. Deuchars, Temporal and spatial properties of local circuits in neocortex. Trends Neurosci. **17**(3), 119–126 (1994)

M. Tsodyks, H. Markram, The neural code between neocortical pyramidal neurons depends on neurotransmitter release probability. Proc. Natl. Acad. Sci. USA **94**, 719–723 (1997)

J. Waters, A. Schaefer, B. Sakmann, Backpropagating action potentials in neurones: measurement, mechanisms and potential functions. Prog. Biophys. Mol. Biol. **87**(1), 145–170 (2005). http://dx.doi.org/10.1016/j.pbiomolbio.2004.06.009. http://www.sciencedirect.com/science/article/pii/S0079610704000653. ISSN 0079-6107. Biophysics of Excitable Tissues

http://www.springer.com/978-3-319-39551-7

Form Versus Function: Theory and Models for Neuronal Substrates

Petrovici, M.A.

2016, XXVI, 374 p. 150 illus., 101 illus. in color.,
Hardcover
ISBN: 978-3-319-39551-7